UNIVERSITY OF MELBOURNE

Ground-Contact Friction Estimation and Slip Prevention in Bipedal Robots

by

Stephen Roosen

Submitted in total fulfilment of the requirements of the degree of Master of Philosophy

in the

Department of Mechanical Engineering

School of Engineering

2012

UNIVERSITY OF MELBOURNE

Abstract

Department of Mechanical Engineering
School of Engineering

Master of Philosophy

by Stephen Roosen

The foot-ground contact force is one of the important factors affecting the gait behaviour, balance and safety of a bipedal robotic mechanism. This force is constrained by the coefficient of friction of the foot-ground contact. This coefficient of friction is thus of high importance, as non-sliding contact and/or the knowledge of the coefficient of friction of the foot-ground contact are common assumptions among bipedal robotics literature. Failure to keep the ratio of the friction force to normal force of the foot-ground contact below the coefficient of friction causes the foot to slip, resulting in a large external disturbance being applied to the biped and causing the bipedal robot to lose balance and fall.

In this work an online estimation technique for estimating the coefficient of friction of the foot-ground contact is developed. It is expected that the estimation algorithm converges to the value of the coefficient of friction of the contact before the ratio of the friction and normal forces exceeds the coefficient of friction, thus allowing the robot control strategy to avoid slipping altogether by altering the forces exerted by the robot actuation. The proposed estimator is validated experimentally using real-world materials. The estimator is shown to be able to determine the coefficient of friction of the materials ahead of the applied force ratio exceeding the coefficient of friction.

Finally a 6-link bipedal robot is modelled and a slip prevention algorithm based on the estimator is implemented to illustrate how a bipedal robot would be able to avoid slipping while walking on a surface of unknown coefficient of friction. The bipedal gait is achieved using a previously developed control algorithm and walks on two flat surfaces of unknown coefficients of friction under ideal simulated conditions. The resulting simulations are compared to demonstrate the effectiveness of the proposed approach. The bipedal robot is shown to be able to walk on a surface of coefficient of friction of 0.4 without slipping and without prior knowledge of this value.

Declaration of Authorship

I, Stephen Roosen, declare that this thesis titled, 'Ground-Contact Friction Estimation and Slip Prevention in Bipedal Robots' and the work presented in it are my own. I certify that:

- The thesis comprises only my original work towards the Master of Philosophy
- Due acknowledgement has been made in the text to all other material used.
- The thesis is less than 50,000 words in length, exclusive of words in tables, maps, bibliographies and appendices.

Signed: _____

Date: _____

Acknowledgements

I would like to thank my supervisor Dr Denny Oetomo for his support, guidance and ideas over the two years.

I would also like to thank Dr Kishor Bhalerao for his expertise and assistance in both mathematical modelling and dynamics simulations.

I would like to thank Mary Galea, Professor of Clinical Physiotherapy, for her assistance in using the motion-capture laboratory at the Royal Talbot Rehabilitation Centre for the experiment.

I would like to thank Dr David Ackland as well as Hossein Mokhtarzadeh for their assistance in performing the experiment.

I would finally like to thank my colleagues in my research group as well as my friends and family for their support over the years.

Contents

List of Figures

Chapter 1

Executive Summary

1.1 Motivation

Since the formulation of the ZMP measure was developed by Miomir Vukobratovic in 1969 [1], research into allowing a bipedal robot to walk in a stable manner gained greater and greater interest in the scientific community, eventually resulting in the unveiling of ASIMO in 2001 (after almost 15 years of top-secret research [2]). Research into bipedal robotics has been approached with many different techniques, ranging from direct measurement of human dynamics [3], dynamic analysis [4], lookahead controllers [5] and PID controllers [6] to fuzzy-logic controllers [7] and neural networks [8]. With extensive research already performed the problem of getting a bipedal robot to walk is no longer a significant goal. Instead the interest has shifted to developing a bipedal robot that can walk robustly, efficiently and adaptively [9].

A key goal of the development of bipedal robots is to create robots that can interact with, and operate alongside of, humans in labour and assistance roles [10]. To realise this goal it is no longer sufficient for bipedal robots to simply operate in a controlled laboratory or specially designed environment, they now need to cope with the wide variety of obstacles that humans deal with on a constant basis: operating in highly variable and often unknown environments as well as responding to unexpected external disturbances.

To achieve this goal extensive research has been committed to developing robust systems spanning a variety of engineering disciplines. Areas of interest include visual and imaging techniques for localisation, mapping and pathfinding [11], optimisation of control algorithms and mechanical designs to improve energy efficiency [12], robust balance control in the face of unknown external disturbances [13], compliant walking for sloped

surfaces [14], rugged surfaces [15], deformable surfaces such as sand or mud and finally low-friction surfaces such as wet or oily surfaces and ice [16–18].

This latter point is interesting. Research into bipedal robots walking on surfaces of arbitrary coefficient of friction has been performed but only for surfaces where the coefficient of friction is known. When the believed value for the coefficient of friction is inaccurate, slip can occur and when it is unknown, the techniques for walking on an arbitrary surface are highly likely to fail. It is this latter condition that is of particular interest in this thesis.

1.2 Overview

The purpose of this thesis is to expand on a bipedal robot's ability to operate in unknown and variable environments, similar to ones that humans would encounter on a regular basis. The phenomenon under study is the coefficient of friction between the foot of the bipedal robot and the walking surface(also known as the ground friction constraint).

Methods for avoiding slip on surfaces of known coefficient of friction as well as compensating for slip if it occurs already exist in literature. The focus in this thesis however is the goal of preventing slip from occurring at all on a surface of unknown and variable coefficient of friction. To the author's knowledge, little research has been performed in this area.

1.3 Problem Statement

The main aim of this study is to develop a friction estimation strategy with the purpose of preventing ground-contact slip for a bipedal robot walking on a surface with unknown coefficient of friction.

Specific aims are:

- Develop a friction model and estimator to estimate ground-contact parameters
- Validate the friction estimator using real-world materials
- Apply the estimator and slip prevention technique to a bipedal robot

1.4 Structure of Thesis

Chapter 2 outlines the background of bipedal robotics and its applications in human society and describes current implementations for balance and control. Current methods for friction estimation and slip compensation and prevention are also outlined.

Chapter 3 proposes a slip-based estimator to estimate the coefficient of friction between the bipedal robot's foot and the walking surface.

An estimator that provides an estimate of the coefficient of friction between the foot and the ground without the need for slip to occur is conceptualised in chapter 4. This involves researching and evaluating friction models, developing the estimation technique and a method for determining convergence.

In chapter 5 the proposed estimator is tested and evaluated using three real-world materials. The results are presented and the performance and efficacy of the estimator is discussed.

In chapter 6 a bipedal robot is modelled and the estimator from chapter 4 is implemented. The purpose of this chapter 6 is to demonstrate the behaviour of the estimator in a slip-prevention algorithm under ideal conditions and is not a main focus of the thesis. Results of the simulation are discussed in chapter 7.

Overall conclusions of the work are presented in chapter 8 and future ideas, goals and developments are suggested in chapter 9.

Chapter 2

Background

2.1 Applications of Bipedal Robots

There are many practical applications for bipedal robots, many of which are only in the conceptual stage. From simple obstacles, to complex unstructured environments, to operating alongside humans in service or assistive roles, bipedal robots will be seeing extensive use in the future.

The bipedal form is a highly versatile mode of transport, able to negotiate terrain that would be impassable to wheeled and multi-legged robots. Bipeds are able to step over small obstacles such as rocks, walk up steep inclines, 'stepping stone' problems where footholds are limited [19], low-traction environments like muddy areas as well as navigate human-developed obstacles such as stairs. These advantages lend bipedal robots the ability to operate in human-oriented environments such as personal homes, offices and factories [20].

This emphasis on mobility in complex and human-like environments allows for a wide array of applications in human assistance and human replacement [21]. Bipedal robots could be utilised in hazardous environments such as maintenance and cleanup in radioactive zones in power plants, fire-fighting and rescue operations in collapsed buildings as part of earthquake response activities or work on construction sites [22, 23]. In military applications, robots could operate in hostile environments, urban combat and mine clearing and in law enforcement applications, could perform bomb disposal activities, similar to roles being performed by robots today but with much greater mobility and versatility. Bipedal robots could also serve as remote proxies for humans, useful for tasks such as geological surveys [24], mining and remote construction as well as exploration and search and rescue activities both in urban and remote areas [25].

Bipedal technology also lends itself to the field of rehabilitation and disability assistance. Bipedal exoskeletons would help with the lower-limb physical therapy for victims of strokes, spine or nerve damage [26], allowing for ongoing therapy outside of specialist facilities and in diverse environments. Paraplegics, quadriplegic and amputees would be able to walk upright instead of using bulky and mobility-limited wheelchairs [27], allowing them to live and navigate without extensive modifications to homes and facilities.

2.2 Friction and Slip

The foot-ground contact friction force is singly responsible for bipedal locomotion as it creates the force required to accelerate and control the biped. The coefficient of friction between the feet of the robot and the ground surface has large effects on the stability, safety and performance of a bipedal robot.

2.2.1 Importance of Friction

In bipedal locomotion the coefficient of friction between the foot and the ground surface determines the maximum acceleration and deceleration of the robot. It constrains the maximum lateral force as well as the maximum control torques [28, 29] that can be applied to a robot. In general, the coefficient of friction directly affects the bipedal robot's stability, its ability to maintain or recover balance due to external disturbances as well as its ability to halt its motion in the event of an emergency.

In the field of ergonomics and biomechanics, much research has been performed to analyse slip and slip induced falling [30, 31] and the effect of friction on slip [32]. The balance, stability, performance and safety of a bipedal robot is greatly affected by its ability to know the coefficient of friction of the surface being walked on. Exceeding this foot-ground coefficient of friction during the robot's operation results in significant disturbance effects and can even cause the robot to lose balance.

2.2.2 Typical Approaches to Handling the Coefficient of Friction

As critical as friction is to bipedal walking it is also highly complex to include in models, simulations and to compensate for. To avoid this complexity, bipedal control algorithms typically assume that the coefficient of friction is never exceeded. This results in one of two approaches.

The first approach is to assume that the the foot-ground coefficient of friction is large enough that the bipedal robot's foot will never slip during operation. This is usually achieved in modelling by assuming that the feet are rigidly fixed to the ground when in contact, modelled by a pin joint at the foot and resulting in a greatly simplified mathematical model. This simplification makes the development of gait controllers much easier as they only need to handle the robot's motion and is the basis of many algorithms [5, 33–36].

The second approach is to assume that the coefficient of friction is finite and thus design a controller that maintains stability by controlling motion but by also introducing constraints on the maximum allowable control torques so that the coefficient of friction is never exceeded. These controllers are usually more complex but have the advantage of being able to successfully operate on a surface where the coefficient of friction is not infinite (although it must be known [18]). Examples can be found in [29, 37, 38].

These approaches require that the coefficient of friction be infinite (never the case) or accurately known (impractical).

2.2.3 Slip Compensation and Low Friction Walking Strategies

For surfaces where the coefficient of friction is known prior to contact but not accurately, a bipedal robot may be able to operate but will occasionally exceed the coefficient of friction, resulting in slip. Since exceeding the coefficient of friction more frequently occurs on surfaces of low coefficient of friction, these cases will be considered as 'low friction' surfaces.

Several strategies have been implemented to allow a bipedal robot to walk on a low-friction surface. The strategies can be roughly separated into slip compensation and slip prevention strategies.

Slip compensation strategies attempt to maintain balance and stability once the coefficient of friction has been exceeded, a condition known as slip, usually via reflex responses.

Boone and Hodgins [39] successfully implemented several reflex strategies to both slipping and tripping in bipedal hopping robots. These strategies were either high-level, pre-programmed responses that would override the main control strategy or would alter low-level control systems such as controller gains until balance was restored.

Park and Kwon [16] implemented several similar reflex slip compensation responses in their bipedal walking robot. The first response was to increase the normal reaction

force (and thus the maximum friction force) at the slipping foot resulting in a vertical acceleration at the hip. This would stop the foot from slipping as long as the hip has sufficient vertical space to translate. The second response was, when slip occurred during the single-stance phase, to shift the swinging leg towards the stance leg however is it not clear how this achieves the desired compensation. The third method is to calculate a 'recovery' trajectory to move the robot from its current configuration back to its original desired trajectory however this was found to only work for small slips. Although successfully implemented, the paper identified that these purely reflex methods have significant limitations that would often be reached for a normal bipedal robot.

Kaneko et al. [40] implemented a 'slip observer' to both detect slip and estimate the slipping force. The paper used the slip force to estimate the moment applied to the bipedal robot's torso due to the slip and thus compensate for and reduce the body roll. This had the effect of reducing the body roll of a bipedal robot walking on a low-friction surface from a peak of 0.04 to approximately 0.02 radians, a 50% improvement however the overall effect of stability was not investigated.

Yamamoto and Ohnishi [17] designed a gait controller that would increase the stride length (and thus the friction force required to walk) each step until it detected slip (done with accelerometers at the feet). The stride length at which slip occurred was then used as an upper limit for the rest of the gait. Their robot was able to successfully walk on a low-friction floor of unknown friction coefficient. Although it was demonstrated to achieve a gait that would not cause slip, this approach required several steps before determining the limit and was only applied on a single surface. It was not investigated how this approach would perform when encountering a transition from one surface to another.

Slip prevention strategies aim to ensure that the coefficient of friction is never exceeded, ensuring that slip never occurs. The advantage of these solutions is that they do not suffer from disturbance effects cause by slip, at the cost of significant algorithmic and computational complexity.

Klein [41] and Nagle [42] both developed solutions to choosing robot joint torques that would satisfy an arbitrary coefficient of friction. Later Kaneko et al. [18] developed a gait controller that would perform on a low-friction surface of approximately known coefficient of friction with minimal disturbance. This work demonstrated a technique to allow bipedal robot to walk on surfaces of arbitrary coefficient of friction by altering its gait and postural behaviour as long as the coefficient of friction is known a priori.

The key difficulty with slip prevention strategies is the requirement that the coefficient of friction be known, or at least conservatively estimated. In these strategies the coefficient

of friction is usually determined experimentally. An error in the assumed value of the coefficient of friction, or if the surface conditions change, would mean that it is not possible to guarantee slip never occurs. A fixed-value strategy also means that the robot is constrained to walk on a particular surface for which its contact friction dynamics with the robot feet has been determined experimentally prior. Therefore, the ability to adapt to a different coefficient of friction is a highly desirable quality for a robot operating in unknown environments.

2.3 Friction Estimation

In the cases where the coefficient of friction is not known prior to contacting the surface, some form of friction estimation may be necessary. The purpose of friction estimation is to identify the value of the coefficient of friction of a surface so that it can be used to identify the constraints on the gait control solution, such as to predict stability margins and maximum control torques. For mobile robots, friction estimation techniques can be divided into two approaches: preemptive friction estimation and feedback friction estimation.

2.3.1 Preemptive Friction Estimation

Preemptive friction estimation attempts to classify the surface before the robot actually makes contact. This can be achieved using laser scanners to determine geometry or video cameras to identify visual features such as surface texture, obstacles and gradients. Research in this area has been performed by Angelova et al. [43] on wheeled robots such as the Mars Rover.

2.3.2 Feedback Friction Estimation

Feedback friction estimation attempts to determine the surface properties once the robot has encountered the new surface. Extensive research has been performed on wheeled vehicles using sensors implanted in the tyres such as stress sensors or acoustic microphones [44] or by correlating the slip ratio of the tyre to friction properties [45] using such models as the Magic Formula tyre model [46].

Although these approaches may work for wheel vehicles, they are inappropriate for use in bipedal robots. Implanted sensors require extensive development, additional sensors, algorithmic complexity and financial expense. Models such as the Magic Formula tyre

model are developed for the particular geometry, material and loading conditions experienced by tyres and so cannot be applied to bipedal robots where foot configuration and loading conditions can vary from implementation to implementation. A 'magic' foot model that could be consistently applied across implementations would make this problem easier to solve but, to the author's knowledge, does not exist. Finally, many of these tyre-slip methods depend on the contact between the tyre and road surface to slip. In a wheeled vehicle with four or more points of contact to the surface, this slip would not cause a large problem, in a bipedal robot however, that has only two points of contact, this could be catastrophic.

To the best of the authors' knowledge, such techniques have not been attempted on bipedal robots in estimating the coefficient of friction of the foot-ground contact.

2.4 Summary

After reviewing the available literature a research opportunity was identified in the field of feedback friction estimation and slip prevention in bipedal robots. The rest of this thesis will explore:

- The possibility of adapting a current technique for slip compensation to provide an estimate of the coefficient of friction
- A novel approach to estimating the coefficient of friction using a friction model
- Validation of the novel approach using real-world materials

The next chapter begins the discussion by looking at a current technique for detection of slip and possible adaptation for the purpose of estimation of the coefficient of friction of the foot-ground contact.

Chapter 3

Slip-Based Friction Estimator

This chapter looks at the development of a slip-based estimator for estimating the coefficient of friction between the ground surface and foot of a bipedal robot. First a technique from Chapter 2, called the Slip Observer, for detecting slip and compensating for the disturbance it causes is reviewed. This technique is then extended to be able to determine the coefficient of friction between the bipedal robot's foot and the ground surface. Finally the issues that may prevent this technique from being optimal are explored.

3.1 Overview of the Slip Observer

To detect and compensate for the destabilising effects of slip Kaneko et al. proposed a Slip Observer [40] to stabilise a bipedal robot walking on a low friction surface.

The Slip Observer estimates the slip force F_{slip} acting at the foot as:

$$F_{slip} = F_{applied} - F_{friction} \tag{3.1}$$

where $F_{applied}$ is the applied force from the ankle joint to the foot in the tangential direction (can be calculated from the biped control routine) and $F_{friction}$ is the ground friction force applied to the foot. Thus the difference between the two is the resultant force acting on the bipedal robot's foot and is called the 'slip force'. Note: Since the friction force cannot be larger than the applied force, F_{slip} cannot be less than zero.

Kaneko et al. used the Slip Observer to detect the occurrence of slip (defined as when $F_{slip} > 0$) and used the slip force to determine the moment applied to the torso due to slip. The observer and compensation was successful in reducing the body roll caused by

the slip force and was able to improve the bipedal robot's stability on a surface with a coefficient of friction of 0.144.

3.2 Extending the Slip Observer

With some extension this Slip Observer could be utilised to work as an estimator for determining the coefficient of friction between the robot foot and ground surface.

This Slip-Based Friction Estimator is as follows:

- When the slip force F_s is equal to zero, then the coefficient of friction cannot be estimated
- When the slip force F_s is not equal to zero, then the coefficient of friction can be estimated as:

$$\mu_c = \frac{F_{friction}}{F_{normal}} \tag{3.2}$$

where F_{normal} is the reaction force normal to the contact surface

3.3 Issues

There are several apparent issues with this estimator.

First, this estimator requires the bipedal robot to slip if the coefficient of friction is to be estimated. In order to maintain balance, slip compensation techniques such as reflex methods [16, 39] would need to be implemented. These reflex methods may not be sufficient to guarantee balance and stability in all cases. Also, slip compensation is designed to stop the bipedal robot slipping, this would prevent the estimator from being able to estimate the coefficient of friction.

Secondly, the estimator does not work when the foot is not slipping. If the gait of the robot is such that the robot never slips (ie. if the coefficient of friction is larger than what is required during normal operation) then the robot could be operating at reduced performance by not taking advantage of the larger lateral forces that could be applied. This could impact efficiency as well as safety should the bipedal robot need to accelerate or decelerate rapidly.

It is preferable that the estimator is able to function without the need for slip to occur.

Chapter 4

Non-Slip Friction Estimator

In chapter 3 a technique for detecting the occurrence of slip reviewed and an estimator for estimating the coefficient of friction was proposed. As outlined in section 3.3, a friction estimator that requires slip to occur is undesirable. The purpose of this chapter is to propose a friction estimator that can estimate the value of the coefficient of friction before slip occurs. For this purpose a model-based estimator will be utilised.

4.1 Requirements of the Estimator

To be effective, the estimator must satisfy the following requirements:

- The estimator must operate online (must update the estimated values during the robot's operation)
- It must operate and the convergence to the estimated value of the coefficient of friction must occur before the actual coefficient of friction is exceeded (ie. during the sticking behaviour)

In order to achieve these requirements our model also must satisfy the following:

- The sticking behaviour must be dependent on the coefficient of friction
- The parameters involved must have physical meaning or represent a measure of physical characteristics

4.2 Choosing a Friction Model

There are two general types of point-contact friction models: *Static models* and *Dynamic models* [47].

Static models attempt to model the sliding and pre-sliding (sticking) behaviours using two separate equations without any internal state variables. Examples of these models are the Classical Models, the Karnopp Model, the Armstrong Model and the Featherstone Model.

The Classical models include the Coulomb, viscous, static friction (stiction) and Stribeck models and combinations of each. To handle the pre-sliding behaviour, the output of these models is simply taken as equal to the applied force. A general form of friction using these classical models is:

$$F_{friction} = \begin{cases} F_{applied} & \text{if } v = 0 \text{ and } -F_s \leq F_{applied} \leq F_s \\ F_c + (F_s - F_c)e^{-|\frac{v}{v_s}|} + F_v v & \text{otherwise} \end{cases} \tag{4.1}$$

where F_c is the Coulomb friction force, F_s is the static friction force, F_v is the viscous friction parameter and v_s is the Stribeck effect parameter. These models exhibit stiction effects when $F_s > F_c$.

These Classical models attempt to model the complex sliding behaviour but fail when the sliding velocity is close or equal to zero due to difficulty in determining when the velocity is zero in an actual simulation or control system. The Karnopp model [48] attempts to remedy the problem of low velocity detection by adding a deadzone to the velocity measurement so when $|v| < \epsilon$ the velocity is taken as zero:

$$F_{friction} = \begin{cases} F_{applied} & \text{if } v < \epsilon \text{ and } -F_s \leq F_{applied} \leq F_s \\ F_c + (F_s - F_c)e^{-|\frac{v}{v_s}|} + F_v v & \text{otherwise} \end{cases} \tag{4.2}$$

This model has a much better performance but the velocity deadzone does not represent real friction behaviour.

A key downside to both the Classical models and the Karnopp model is that they do not model the sticking behaviour. They instead require the applied force as an input to the system, a variable that is not always explicitly given.

The Armstrong model [49] is one of the first models to investigate the sticking behaviour of dry friction. Armstrong's analysis showed that the sticking behaviour exhibits elastic deformation up until a maximum displacement at which the static friction force F_s is attained. The Armstrong model replaces the Classical models' approach to sticking with a spring model:

$$F_{friction} = \sigma_0 x; \quad \text{for } -F_s \leq \sigma_0 x \leq F_s \tag{4.3}$$

where σ_0 is the stiffness of the system and x is the contact displacement.

A model by Featherstone [50] uses a spring-damper model instead of a single spring to model Coulomb friction with sticking behaviour. It is expressed as:

$$F_{friction} = \begin{cases} \mu F_{normal} & \text{if } F_{stick} > \mu F_{normal} \\ F_{stick} & \\ -\mu F_{normal} & \text{if } F_{stick} < -\mu F_{normal} \end{cases} \tag{4.4}$$

where $F_{stick} = -kx - b\dot{x}$ and μ is the coefficient of kinematic (Coulomb) friction. These models, although modelling the sticking behaviour, are still discontinuous and the switching parameter μ is part of the slip equation, not the sticking equation.

The inability to determine the switching parameter threshold during the sticking behaviour means that these static friction models cannot be used for our purposes.

Dynamic models use a single, continuous equation to model both the sticking and sliding behaviour, usually by containing internal state variables. The earliest example of these models is the *Dahl model* [51]. The Dahl model was inspired by the stress-strain curve from classical solid mechanics. As a force is applied the friction force increases until reaching rupture. Dahl modelled the stress-strain curve by a differential equation:

$$\frac{dF_{friction}}{dx} = \sigma(1 - \frac{F_{friction}}{F_c} sgn(\dot{x}))^{\alpha} \tag{4.5}$$

Which can also be expressed in the time domain:

$$\frac{dF_{friction}}{dt} = \frac{dF_{friction}}{dx}\frac{dx}{dt} = \sigma(1 - \frac{F_{friction}}{F_c} sgn(\dot{x}))^{\alpha}\ \dot{x} \tag{4.6}$$

where σ is the contact stiffness, F_c is the Coulomb friction and $\dot{x}$ is the relative velocity of the two surfaces in contact. This model is a generalisation of Coulomb friction with

sticking behaviour. It does not model velocity-dependant phenomena such as Stribeck or Viscous friction.

Other models exist that add static friction and velocity-dependent phenomena (ie. Stribeck friction) such as the *LuGre* and *Bliman-Sorine* models.

The LuGre model [52] was developed using the 'bristle model' interpretation of friction where the friction force is caused by elastic deflection of surface springs. When the friction force is large enough the bristles rupture, resulting in slip. The model has the form:

$$\frac{dz}{dt} = \dot{x} - \sigma_0 \frac{\dot{x}}{g(\dot{x})} z \tag{4.7}$$

$$F_{friction} = \sigma_0 z + \sigma_1 \frac{dz}{dt} + f(\dot{x}) \tag{4.8}$$

where z is the average bristle deflection, $g(\dot{x})$ models Stribeck friction behaviour, $f(\dot{x})$ models the Viscous friction behaviour and σ_0, σ_1 are parameters.

There are several issues that make this model unsuitable for our purposes. First, arbitrary functions for $g(\dot{x})$ (the non-slip behaviour) and $f(\dot{x})$ (the viscous behaviour) need to be selected so that they are both realistic without being overly complex. Second, the number of parameters required to fit the model $(\sigma_0, \sigma_1, f(\dot{x}), g(\dot{x}))$ would make the estimator more difficult to design and tune. Finally, the parameters in the model do not have direct physical meaning.

Bliman and Sorine [53] used the theory of hysteresis operators [54] to develop a family of dynamic models that are simple, efficient and can at the same time model the sticking and sliding behaviours as well as static friction, Stribeck and Coulomb friction. The first model is a first order model that only models coulomb friction, it is a particular case of the Dahl model (4.2) with $\alpha = 1$:

$$\frac{dF}{dx} = \frac{-3sgn(\dot{x})}{s_p} F + \frac{3F_c}{s_p} \tag{4.9}$$

and in the time domain:

$$\frac{dF}{dt} = \frac{-3|\dot{x}|}{s_p} F + \frac{3F_c}{s_p} \dot{x} \tag{4.10}$$

where F_c is the Coulomb friction force and s_p is the approximate displacement at which the friction saturates (ie. when $F = F_c$,see Fig 4.1).

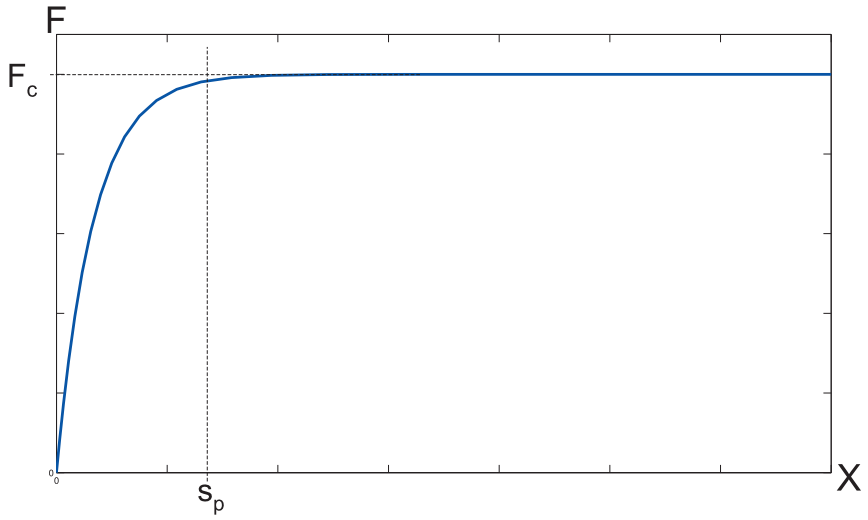

FIGURE 4.1: First Order Bliman-Sorine Model

A second order model includes static friction as well as pseudo-Stribeck friction. It is a linear combination of a fast and a slow first order model.

$$\dot{z} = \begin{bmatrix} -1/\epsilon_f\eta & 0 \\ 0 & -1/\epsilon_f \end{bmatrix} |\dot{x}|z + \dot{x} \begin{bmatrix} f_1/\epsilon_f\eta \\ -f_2/\epsilon_f \end{bmatrix} \tag{4.11}$$

$$F_{friction} = \begin{bmatrix} 1 & 1 \end{bmatrix} z$$

where $z_{2\times1}$ are the internal states of the model and f_1, f_2, ϵ_f and η are parameters such that:

$$\begin{aligned} F_c =& f_1 - f_2 \\ F_s =& F_c + 2f_2(1-\eta)(\frac{\eta f_2}{f_1})^{\eta/(1-\eta)} \\ s_e =& \frac{\epsilon_f\eta}{1-\eta} ln(\frac{f_1}{\eta f_2}) \\ s_p =& 3\epsilon_f \end{aligned}$$

where F_c is the Coulomb friction force, F_s is the static friction force, s_e is the approximate displacement at which the system begins to slip (ie. when $F = F_s$) and s_p is the approximate displacement at which $F = F_c$ (see fig 4.2). It should be noted that the Stribeck effect in this model is not true Stribeck friction as it is not dependent on velocity.

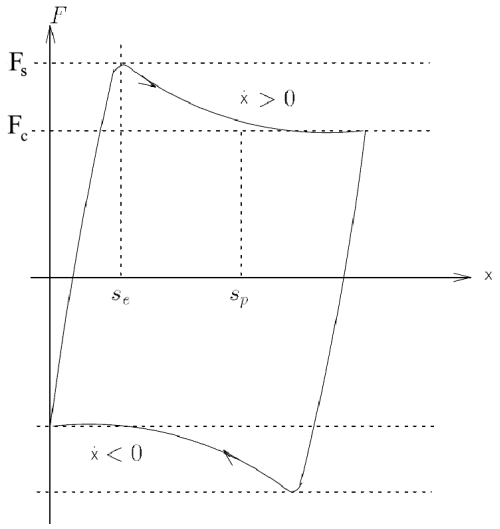

FIGURE 4.2: Second Order Bliman-Sorine Model [53]

A second order model is much more complex to fit to data than a first order model. The number of parameters involved means that there are many degrees of freedom in the model, requiring the derivative of two state variables increases the estimator's sensitivity to noise. Finally the state variables z are not directly measurable and may not be observable. Although fitting the model manually by inspection may be feasible, using an parameter estimation technique to do so may not be.

The first order Bliman-Sorine model is in fact appropriate for our purposes. This model is suitable for several reasons:

- It is continuous from the sticking to the sliding behaviours
- It has low complexity with few parameters to deal with (F_c and s_p)
- The parameters have physical meaning (the maximum friction force F_c is explicit in the model)
- The sticking behaviour is dependent on the coefficient of friction
- The model can be represented as linear with respect to the parameters to be estimated (see section 4.4)

Obvious issues of the first order model include:

- It does not model Stribeck or viscous effects. This is acceptable since the main concern is with the sticking behaviour of the model, which dominates at low slip velocities. In order for Stribeck or viscous effects to become significant the robot's

foot must be slipping at a (relatively) large velocity. In this case the system can be considered to have failed, as the purpose of the estimator is to prevent slip entirely.

- The model contains the state variable F. This will complicate aspects such as data acquisition and noise robustness but this issue is unavoidable without reverting to a static model.

There are two other limitations that occur when using this model in simulation:

- The model introduces unrealistic oscillation effects when the applied force is low.
- The model does not guarantee that $F_{friction} < F_{applied}$.

These effects arise due to the model being a hysteresis model combined with a discrete step-solver. In this work the model is being used as estimator and so these limitations should not apply.

A key problem with this model is that the parameter F_c is dependent on the normal contact force ($F_c = \mu_c F_n$). Singularities occur when the normal force is close to zero. In this form the model is inappropriate to use due to the fact that the normal contact force frequently changes during the bipedal gait. Thus the model cannot be used in its current form.

The solution to this problem is to modify the model into a form that does not depend on the normal force. This can be achieved by normalising the model with respect to the normal force. This results in a model that represents the coefficient of friction rather than the friction force itself:

$$\dot{u} = \frac{-3|\dot{x}|}{s_p} u + \frac{3\mu_c}{s_p}\dot{x} \tag{4.12}$$
$$F_f = uF_n$$

where $\dot{x}$ is the relative tangential velocity of the contact point, μ_c is the coefficient of kinematic (coulomb) friction and s_p is an estimate of the displacement before the friction reaches saturation (as before). Here u is a state variable representing the normalised friction state.

The model described in equation 4.2 now satisfies all our requirements from section 4.1.

An appropriate friction model is only half of the estimation problem, the next section will outline an appropriate estimation algorithm.

4.3 Overview of The Recursive Least Squares Algorithm

The role of this section is to develop an estimator algorithm to update the estimates of the parameters μ_c and s_p in our chosen friction model.

Estimators are frequently used in control systems to determine the values of internal state variables in a model, usually to filter noisy measurements or determine the values of states where direct measurements are unavailable or infeasible. However estimators are not limited to estimating states, they can also be used to estimate internal model parameters. It is the latter approach that is useful for this estimator.

For this purpose a parameter estimation technique known as Least Squares Estimation will be used.

Curve fitting by minimisation of the sum of squared-error (least squares error) is a common technique in data analysis. For the purposes of system identification it can be used to identify system parameters based on measured data. For online estimation purposes, the algorithm can be performed recursively to dynamically update the parameter estimates as data is acquired. The simplest implementation requires the model to be linear with respect to its parameters and is the one that will be outlined here. Although techniques exist for models with non-linear parameters [55], they are more complex to implement and were not required since the model selected is linear.

An arbitrary linear function:

$$y(t) = a_1x_1(t) + a_2x_2(t) + \cdots + a_nx_n(t) + b_1u_1(t) + b_2u_2(t) + \cdots + b_mu_m(t)$$

When sampled discretely, it becomes:

$$y[k] = a_1x_1[k] + a_2x_2[k] + \cdots + a_nx_n[k] + b_1u_1[k] + b_2u_2[k] + \cdots + b_mu_m[k]$$

This can be represented as:

$$y_k = \theta_k^T r_k \tag{4.13}$$

where:

$$\theta_k = \begin{bmatrix} a_1 & \cdots & a_n & b_1 & \cdots & b_m \end{bmatrix}^T \tag{4.14}$$

is the vector containing the parameters of the model, and:

$$r_k = \begin{bmatrix} x_1[k] & \cdots & x_n[k] & u_1[k] & \cdots & u_m[k] \end{bmatrix}^T \tag{4.15}$$

is the vector of current measured inputs (known as the regression vector) and y_k is the current measured output.

The algorithm contains two internal variables that need to be initialised. The initial parameter estimate vector θ_0 is set to the initial estimates of each parameter $\theta_0 = [a_0 b_0]^T$. The covariance matrix P is a diagonal matrix representing the confidence in the current parameter estimates. When P_k is zero (or close to zero), the parameter estimates will not be updated by data measured at time instant k. For this reason the covariance matrix is initialised to a large value.

The steps to perform the Recursive Least Squares Estimation Algorithm are as follows:

- Step 0: Set the parameter estimates θ and covariance matrix P to their initial values
- Step 1: calculate the error between the currently measured output and the estimated output based on current estimations of θ

$$e_k = y_k - \theta_k^T r_k \tag{4.16}$$

- Step 2: Calculate the gain matrix K

$$K = \frac{P_k r_k}{\lambda + r_k^T P_k r_k} \tag{4.17}$$

- Step 3: Update the estimate of θ

$$\theta_{k+1} = \theta_k + K e_k \tag{4.18}$$

- Step 4: Update the covariance matrix P

$$P_{k+1} = \frac{1}{\lambda}(I_{m+n \times m+n} - K r_k) P_k \tag{4.19}$$

- Go to step 1 at the next cycle

The parameter λ is known as the forgetting factor and controls the influence that previous measurements have on the current estimate. Typical values for λ are between 0.9 to 1.0. A high value results in greater robustness to noise at the cost of convergence and parameter tracking response and a lower value results in improved speed of convergence at the cost of increased sensitivity to noise.

4.4 Formulation of Regression Model

For our purposes the Recursive Least Squares (RLS) Algorithm will be used to estimate the coefficient of friction μ_c. In order to do this it is required that the estimator model be in a form that is linear with respect to its parameters. The regression vector r_k, the parameter vector θ_k and the output y_k must then be identified.

The model selected in section 4.2 was partly chosen due to the ease with which it can be rearranged.

$$\begin{aligned} \dot{u} &= \frac{-3|\dot{x}|}{s_p}u + \frac{3\mu_c}{s_p}\dot{x} \\ F_{friction} &= uF_{normal} \end{aligned} \tag{4.20}$$

The variables are:

- $\dot{x}$: The relative velocity of the sliding surfaces
- u: The current friction state (ratio of the current friction force to normal force), $u = \frac{F_{friction}}{F_{normal}}$
- μ_c: The coefficient of friction - the maximum ratio that u can achieve. When $F_{applied} < \mu_c F_{normal}$ the surfaces undergo elastic deformation and displace sightly relative to each other. When $F_{applied} \geq \mu_c F_{normal}$ the surfaces will slide. This transition is continuous.
- s_p: Approximate displacement at which the friction saturates (ie. when $u = \mu_c$)

Equation 4.4 can be rearranged into:

$$y = a_1 x_1 + a_2 x_2 \tag{4.21}$$

where:

$$y = \dot{u} \tag{4.22}$$

$$x_1 = |\dot{x}|u \tag{4.23}$$

$$x_2 = \dot{x} \tag{4.24}$$

$$\tag{4.25}$$

$$a_1 = \frac{-3}{s_p}$$

$$a_2 = \frac{3\mu_c}{s_p} \tag{4.26}$$

The regression vector is:

$$r_k = \begin{bmatrix} |\dot{x}|u \\ \dot{x} \end{bmatrix} \tag{4.27}$$

The parameter vector is:

$$\theta_k = \begin{bmatrix} a_1 \\ a_2 \end{bmatrix} \tag{4.28}$$

After the RLS loop the parameters can be determined as:

$$\mu_c = -\frac{a_2}{a_1} \tag{4.29}$$

$$s_p = -\frac{3}{a_1} \tag{4.30}$$

4.5 Parameter Convergence

The final piece of the friction estimator algorithm is the matter of determining when the estimation has converged to its final value. Failing to do so could result in an inaccurate estimate of the coefficient of friction.

This is done by monitoring the Least Squares Estimate error e_k after each time step to see if the magnitude of this error has reduced to below a set threshold for a set number of consecutive time steps.

This can be expressed as:

$$n_k = \begin{cases} n_{k-1} + 1 & \text{if } |e_k| < \epsilon \\ 0 & \text{otherwise} \end{cases} \tag{4.31}$$

and the convergence flag a is set such that:

$$a = \begin{cases} 1 & n_k \geq N \\ 0 & \text{otherwise} \end{cases} \tag{4.32}$$

where n is the number of samples where the estimate error e_k is within the threshold ϵ and N is the number of samples required to be within the threshold before the estimation is taken as having converged to a value.

4.6 Friction Estimator Algorithm

With the RLS Algorithm and an appropriate regression model the general Friction Estimator Algorithm can now be outlined.

In order to perform the algorithm the estimator inputs that need to be measured must be identified:

- $\dot{x}$: The foot velocity tangential to the contact surface
- F_n: The contact force normal to the contact surface
- F_x: The contact force tangential to the contact surface

The overall process of the non-slip friction estimator proceeds as follows. For each servo loop:

- Step 1: Determine the foot velocity $\dot{x}$ either by forward kinematics of the robot or by integration of an accelerometer placed at the foot (or a combination of the two)
- Step 2: Determine the foot reaction forces and calculate the current state variable u as $u = \frac{F_x}{F_n}$
- Step 3: Create the regression vector $r_k = \begin{bmatrix} |\dot{x}|u \\ \dot{x} \end{bmatrix}$
- Step 4: Derive u to get the current state variable $\dot{u}$ to obtain the output $y = \dot{u}$
- Step 5: Perform the Recursive Least Squares algorithm loop from section 4.3
- Step 6: Update the current estimate of the coefficient of friction: $\mu_c = -\frac{b}{a}$

- Step 7: Check convergence conditions (section 4.5) and notify high-level controller if conditions have been met
- Step 8: Repeat steps 1 to 7 for the other foot

4.7 Summary

In this chapter an estimator for determining the coefficient of friction between two surfaces without slipping was established. In chapter 5 the estimator will be applied to three real-world materials and the effectiveness validated.

Chapter 5

Experimental Validation of Proposed Estimator

To validate the effectiveness of the proposed estimation scheme, an experiment was carried out to obtain the force, displacement and velocity profiles of a mass in contact with the ground when an external force is exerted along the horizontal direction. Multiple surface-contact conditions were investigated.

The purpose of this experiment is to validate the behaviour of the non-slip friction estimator and estimate the parameters of a physical system. This involved a physical data-collection exercise where external forces were introduced to the mass-ground system until gross slip occurred. This data was then processed by the algorithm in an offline manner.

5.1 Experimental Setup

5.1.1 Overview

The experiment is designed to acquire force and velocity data of two surfaces in non-sliding (sticking) contact as an external driving force is applied. This should allow the behaviour of friction during non-sliding contact to be quantified and used in the non-slip friction estimator. To achieve this a rig was fabricated and force and position data was measured.

5.1.2 Friction Test Rig

The rig is designed to study the behaviour of friction between two surfaces moving tangentially to each other in contact. The moving body (Body 1) was a steel block (height = 150mm, width = 150mm, length = 200mm, mass = 5.05kg) and attached to a rope, reflective spherical markers were mounted to the four corners of the block to enable the absolute position of the block to be measured. Body 2 is the ground surface, in this case a steel VICON force plate. A material under investigation was placed between the two bodies and fixed to body 1. The three materials investigated were neoprene, rubber and mattress foam.

The data measured was the absolute position of the centre of mass of body 1, the normal contact force between body 1 and body 2, and the lateral forces between body 1 and body 2.

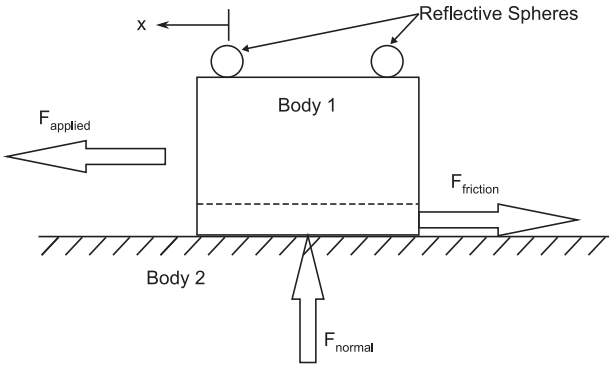

FIGURE 5.1: Friction Test Rig

5.1.3 Force and Position Data

The rig position and ground reaction force data was measured using a VICON motion capture system. The VICON system uses 8 video cameras arranged around a workspace that are calibrated to detect four highly-reflective spherical markers placed on the rig. The VICON software combines the imagery from the cameras to accurately determine the three dimensional location of each sphere within the workspace coordinates. The VICON system also includes several high-range, high-resolution force plates to measure contact forces and moments in all three dimensions. Since the position and force measurements are measured by the same system, the resulting data is synchronised together, so no further synchronisation processes are required.

The force-plate that will represent the ground in this experiment is made of steel.

5.2 Experimental Procedure

The experiment was performed by placing the rig on the VICON force plate and applying a ramp drag force to the rig by pulling on the attached rope. Once the rig entered the gross slip phase the applied force was removed.

The raw motion-capture data was extracted using a Matlab library. The velocity of body 1 was obtained by differentiating the average position of the four markers. The position and force data were both low-pass filtered prior to differentiating to remove high-frequency noise. The selected cutoff frequency was tuned to be 3.54Hz.

The data was then processed using the proposed algorithm (section 4.6). The results and discussion are presented in the following section.

5.3 Results

In the following section only the estimate of the coefficient of friction was reported. Although the parameter s_p was estimated, the value of the parameter is not of interest in the prevention of slip and so is ignored.

Several tests were performed for each surface contact. Each test successfully converged to the final estimated value before the rig slipped. Discussed below is a representative sample of each contact condition.

For the convergence flag: the value of N was chosen by trial and error and was constant for all tests. This value can be increased to achieve a more aggressive estimate, or decreased to achieve a more conservative estimate of the coefficient of friction.

The value of the normal contact force is not shown as only the ratio of the contact friction force to normal force is of interest in the estimation strategy. For reference the value of the normal force was constant at 49.5N. Noise in the measurement system was responsible for high frequency fluctuations of ±4N. This noise was removed by low-pass filtering (see above).

5.3.1 Neoprene-Steel Contact

This sub-section presents the results for the test case using a sheet of neoprene (20mm thick) as the material under investigation. As a ramp force input was applied the ground reaction forces and velocity of body 1 were measured. Figures 5.2 to 5.5 present the

ratio of ground reaction forces, the velocity of body 1, the result of the non-slip friction estimator and the superimposition of the velocity and friction estimator respectively.

Figure 5.2 shows the ratio of the ground friction force to the normal force (known as the current friction state).

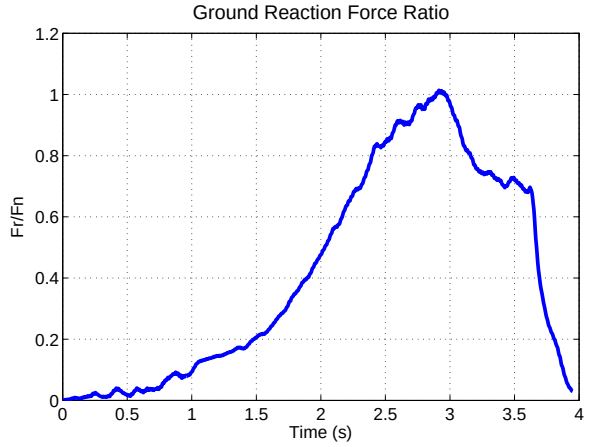

FIGURE 5.2: Friction State

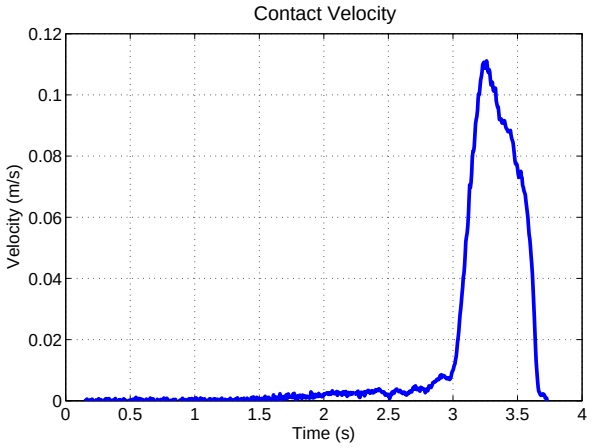

FIGURE 5.3: Velocity of Mass-Ground Contact

From $t = 0s$ to $t = 2.9s$ a ramp force is applied. At $t = 2.9s$ the ground force ratio reaches the coefficient of static friction at $\mu_s = 1$ and body 1 begins to slip. From $t = 2.9s$ to $t = 3.5s$ the ground force ratio decayed to the value of the coefficient of Coulomb friction at $\mu_c = 0.75$. At $t = 3.5s$ the applied force is removed and body 1 returns to rest.

Figure 5.3 shows the velocity of body 1. It can be observed that body 1 remains at rest from $t = 0s$ until slip occurs at $t = 2.9s$. When slip occurs the velocity of body 1 rapidly increases before returning to rest after the applied force is removed at $t = 3.5s$.

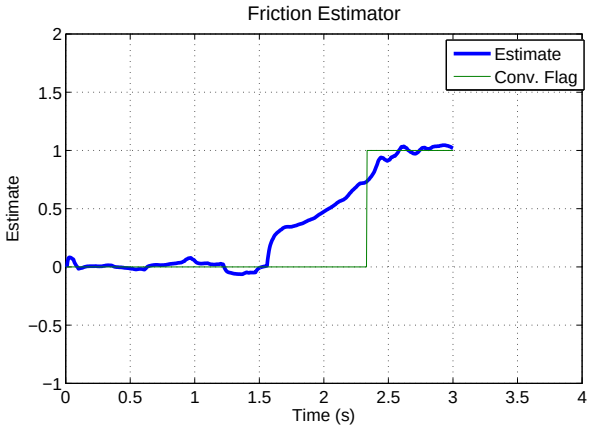

FIGURE 5.4: Friction Estimator

Figure 5.4 shows the state of the non-slip estimator as it converges to the estimate of the coefficient of static friction. The estimator achieves its steady state value of 1.0 at $t = 2.5s$, $0.4s$ before the ground force ratio reaches the coefficient of static friction.

The convergence flag a (see section 4.5) goes to 1 at $t = 2.3s$ to notify that the estimator has sufficiently converged to its final value. The flag can be tuned to trigger at an earlier point in time to achieve a more conservative estimate for μ, or later for a more aggressive estimate.

Figure 5.5 shows the result of the friction estimator superimposed on the velocity of body 1. It can be clearly observed that the friction estimator converges to an estimate of the coefficient of friction (approximately 1.0) $0.4s$ before gross slip occurs.

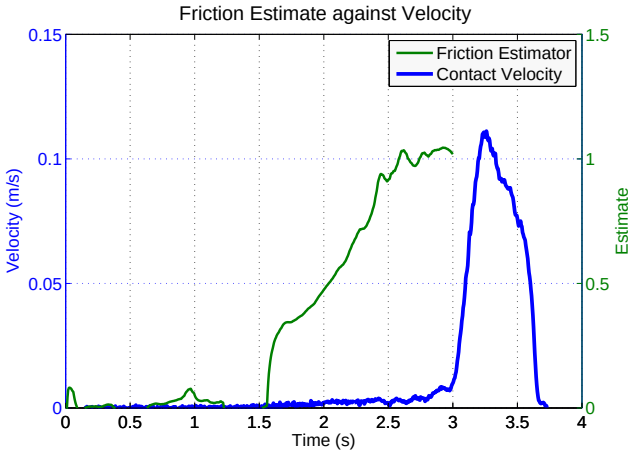

FIGURE 5.5: Friction Estimator against Contact Velocity

5.3.2 Rubber-Steel Contact

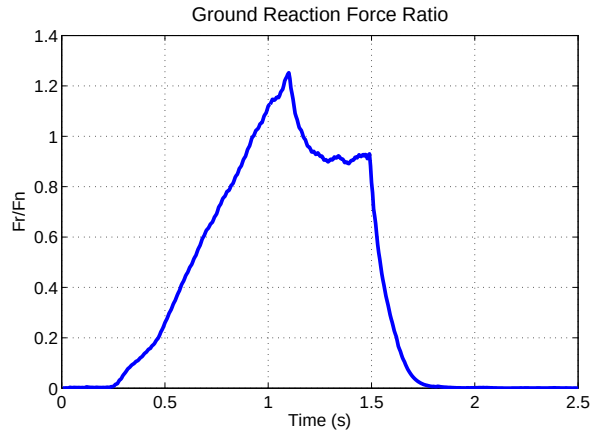

FIGURE 5.6: Friction State

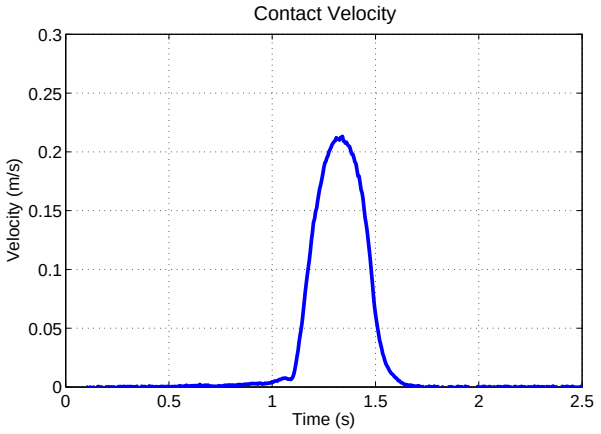

FIGURE 5.7: Velocity of Mass-Ground Contact

From figure 5.6, a ramp force is applied from $t = 0.25s$ to $t = 1.1s$. The coefficient of static friction of $\mu_c = 1.25$ is achieved at $t = 1.1s$. Once slip occurs the ground reaction force ratio decayed to the coefficient of Coloumb friction of $\mu_c = 0.93$ at $t = 1.25s$. The applied force is removed at $t = 1.5s$.

Figure 5.7 shows the velocity of body 1. It can be observed that body 1 remains at rest from $t = 0s$ until slip occurs at $t = 1.1s$. When slip occurs the velocity of body 1 rapidly increases before returning to rest after the applied force is removed at $t = 1.5s$.

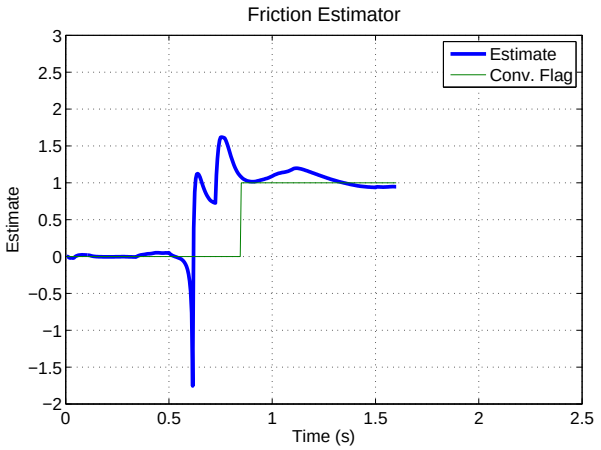

FIGURE 5.8: Friction Estimator

Figure 5.8 shows the results of the non-slip estimator. The estimator achieves its steady state value of about 1.1 at $t = 0.85s$, $0.25s$ before the ground reaction force ratio reaches the coefficient of static friction. Here the estimator does not converge exactly to the value of the coefficient of static friction of 1.25 but does converge to a value slightly below. Most importantly it does not exceed the coefficient of static friction.

Figure 5.9 shows the result of the friction estimator superimposed on the velocity of body 1. It can be clearly observed that the friction estimator converges to an estimate of the coefficient of friction (approximately 1.25) $0.25s$ before gross slip occurs.

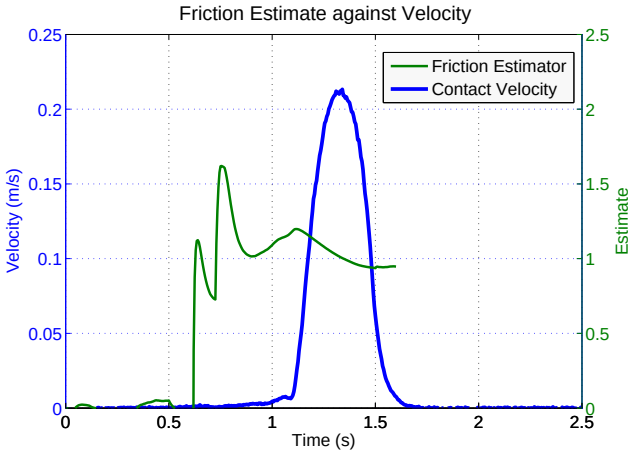

FIGURE 5.9: Friction Estimator against Contact Velocity

5.3.3 Foam-Steel Contact

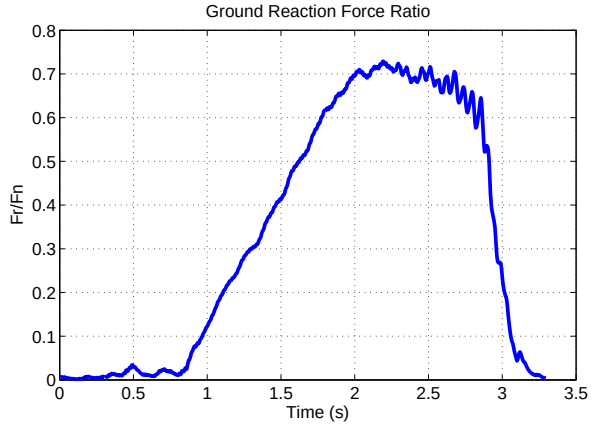

FIGURE 5.10: Friction State

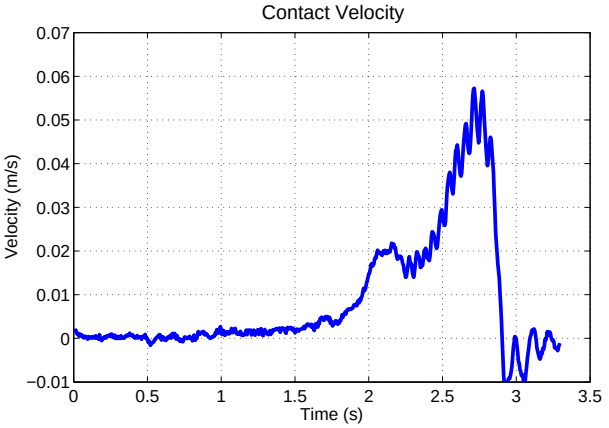

FIGURE 5.11: Velocity of Mass-Ground Contact

From figure 5.10, A ramp force is applied from $t = 0.7s$ to $t = 2.4s$ at which the coefficient of static friction of $\mu_c = 0.72$ is achieved. There is little difference between the coefficient of Coloumb friction and the coefficient of static friction. The applied force is removed at $t = 2.7s$

Figure 5.11 shows the velocity of body 1. It can be observed that body 1 remains at rest from $t = 0s$ until slip occurs at $t = 2.4s$. When slip occurs the velocity of body 1 rapidly increases before returning to rest after the applied force is removed at $t = 2.7s$.

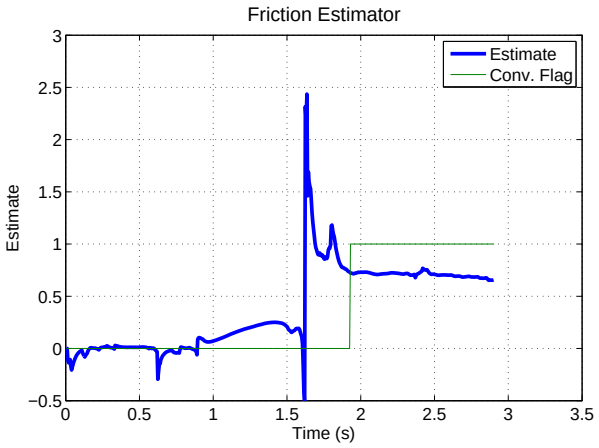

FIGURE 5.12: Friction Estimator

Figure 5.12 shows the non-slip estimator. The estimator achieves its steady state value of about 0.7 at $t = 0.95s$, $0.45s$ before the friction force reaches the coefficient of static friction.

Figure 5.13 shows the result of the friction estimator superimposed on the velocity of body 1. It can be clearly observed that the friction estimator converges to an estimate of the coefficient of friction (approximately 0.7) $0.45s$ before gross slip occurs.

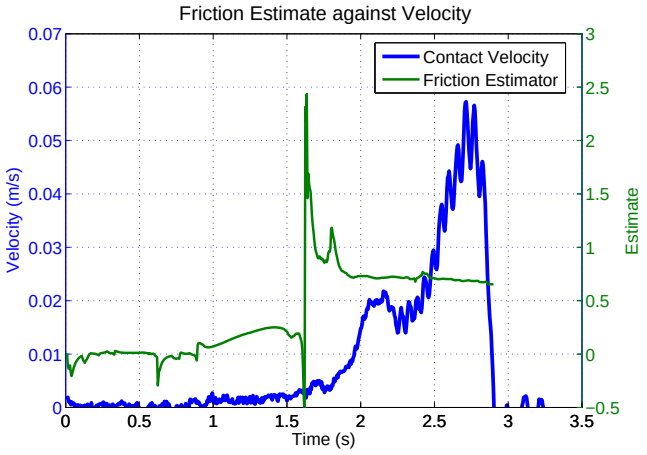

FIGURE 5.13: Friction Estimator against Contact Velocity

5.4 Discussion

The results show that a first-order estimator can determine the coefficient of friction between two surfaces before slip occurs.

Several issues that would affect the performance of the estimator were identified:

- Sensitivity and resolution of the position and force measurements
- Rate at which the data is acquired
- Rate of application of applied load
- Choice of N for the convergence flag

These issues were not investigated but instead left to future research.

This estimator allows a bipedal robot to have knowledge of the ground friction constraint during walking instead of requiring a pre-determined or assumed value. The robot would also be able to respond to a new surface where the friction constraint changes.

This solution will allow a robot to determine when it is close to exceeding the coefficient of friction, with sufficient time to alter its internal torque profile to prevent slipping from occurring and thus maintaining balance at all times. The identified coefficient of friction can also be passed to the high-level motion planning algorithm to dynamically adjust the gait behaviour, resulting in enhanced performance, efficiency, balance and safety.

Chapter 6

Simulation of Bipedal System

In this chapter the non-slip friction estimator is implemented in a bipedal robot simulation. A 6-link bipedal robot, ground reaction forces and input torques is simulated and a basic slip prevention algorithm is implemented to illustrate an application of the non-slip friction estimator.

6.1 Dynamic Model of Bipedal Robot

A simplified bipedal robot model was constrained to operating in the sagittal plane, a common technique in biped gait synthesis and analysis. The bipedal robot was designed with point feet instead of ankles. This provided simplification to the simulation however it limits the availability of gait algorithms, preventing the use of algorithms that rely on multiple contact points at each foot, such as Zero-Moment Point based methods. This results in a 4-link bipedal model: two femurs (upper legs) and two tibias (lower legs) actuated by four joints (two hip joints, two knee joints) each modelled as a single degree of freedom revolute joint.

Neither foot was assumed to be fixed to the ground. This was achieved by adding a floating-base to the centre of mass (M_{body}) of the robot to allow for free vertical and horizontal translation (links q_0 and q_1 in figure 6.1). A floating base consists of two 'virtual' prismatic joints (x and y translation), each having no mass and are unactuated since they have no real physical existence. The floating base adds two joints to the bipedal robot model resulting in a total of six joints. The bipedal robot model is shown in figure 6.1. Variables q_0 and q_1 are the cartesian x and y position, q_2 is the angle of hip joint 1, q_3 is the angle of hip joint 2, q_4 is the angle of knee joint 1 and q_5 is the angle of knee joint 2.

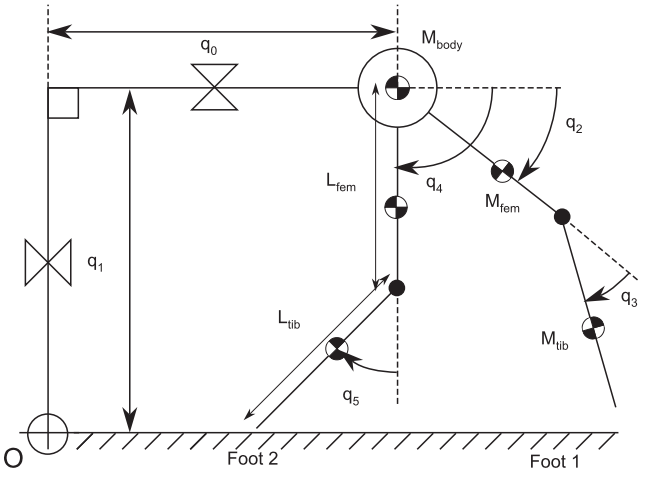

FIGURE 6.1: Bipedal Robot Model with Floating Base

Five masses are defined: a mass at each femur (M_{fem}) and tibia (M_{tib}) and a larger (dominant) mass to represent the combined mass of the torso (M_{body}).

The simulation was performed using a Dormand-Prince [56] ordinary differential equation solver (known as ode45() in Matlab). The dynamics of the system are as follows:

$$M(q)\ddot{q} + C(\dot{q}, q) + G(q) = \tau_i + J_1^T F_1 + J_2^T F_2 \tag{6.1}$$

where $q = [q_0, q_1, q_2, q_3, q_4, q_5]^T, \dot{q} = \frac{dq}{dt}$ and $\ddot{q} = \frac{d\dot{q}}{dt}$. The inertia matrix M, Coriolis and centrifugal vector C and gravity vector G are given in Appendix A. F_1 and F_2 are the ground reaction forces at Foot 1 and Foot 2 and J_1, J_2 (see figure 6.2) are the jacobian matrices that map the joint velocities to the velocities of each foot (also in Appendix A). τ_i is the inputs from the controller. Note: since links q_0 and q_1 are virtual links, τ_0 and τ_1 must equal zero.

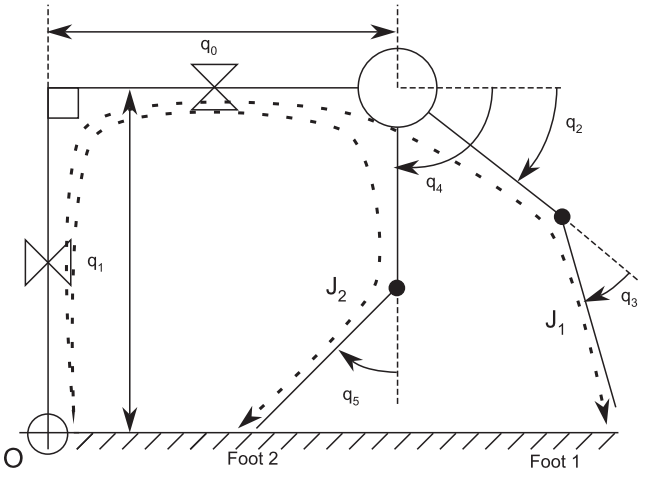

FIGURE 6.2: Bipedal Robot Model showing Jacobians

In this chapter 'Foot 1' is defined as the foot made up of the kinematic chain q_0, q_1, q_2, q_3, 'Foot 2' is defined as the foot made up of the kinematic chain q_0, q_1, q_4, q_5 (see figure 6.1). During the double-stance phase (when both feet are in contact with the ground) the 'Front Foot' (subscript 'F') is the foot with the greater positive x position and the 'Rear Foot' (subscript 'R') is other the foot. During the single-stance phase (when only one foot is in contact with the ground ie. when the bipedal robot is stepping) the 'Stance Foot' (subscript 'st') is the foot in contact with the ground and the 'Swing Foot' (subscript 'sw') is the foot in motion (see figure 6.3).

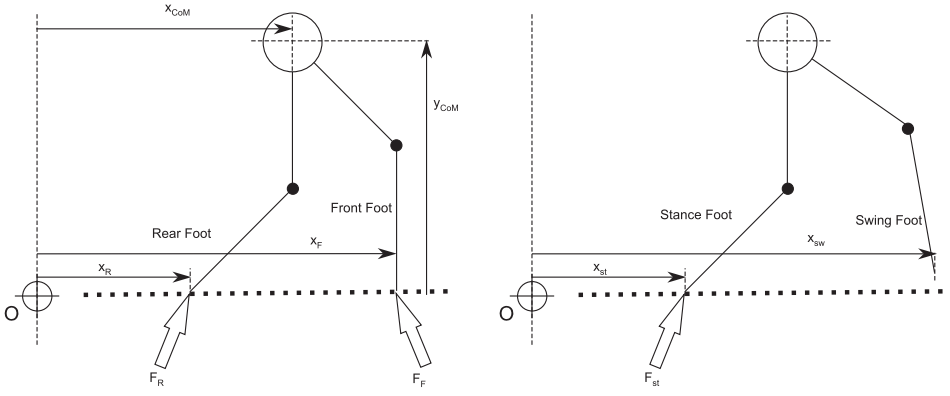

FIGURE 6.3: Bipedal Robot Model showing Subscripts

6.2 Modelling of Contact Surface

The contact model can be separated into two models, the normal force contact model (impact model) and the tangential force contact model (friction model).

6.2.1 Impact Model

The normal and impact force model used is a non-linear spring-damper model based on the work of Hunt and Crossley [57]. This model was chosen because there are no discontinuities at the point of impact as well as being realistic, although it can be stiff depending on the parameters chosen.

The model is described as:

$$F_n = ky^n + by^p\dot{y}^q \tag{6.2}$$

where F_n is the normal force, y is the penetration depth, k is the spring constant, b is the damping constant and n, p, q are the parameters to model the non-linear behaviour.

The values chosen for our simulation were $k = 50000$, $b = 35000$ and $n = p = q = 1.0$. These values are similar to other values found in literature and so are considered to be realistic [58, 59].

6.2.2 Friction Model

To simulate the friction between the robot foot and walking surface a first-order Bliman-Sorine model was used:

$$\begin{aligned} \dot{u} &= \frac{-3|\dot{x}|}{s_p}u + \frac{3\mu_c}{s_p}\dot{x} \\ F_f &= uF_n \end{aligned} \tag{6.3}$$

The value s_p is usually in the order 10^{-3} and so the system is stiff. The stiffness of the system combined with the use of the non-stiff Dormand-Prince solver results in some noise in the simulated result.

The purpose of the Chapter 5 was to prove that the first-order Bliman-Sorine model was a feasible estimator when applied to more complex, higher-order friction phenomena such as found in real-world surfaces. Since the biped model is intended to be illustrative in the use of the slip prevention algorithm rather than the accuracy of the friction estimator, the first-order Bliman-Sorine model was used to make the simulation faster and more reliable.

6.3 Sensor and Actuator Modelling

For the purposes of simulation it is assumed the robot has access to ideal sensors so that joint location and velocity as well as ground contact forces are all accurately known. To simplify the simulation, sensor dynamics were not modelled.

It is also assumed that ideal actuators are used so actuator dynamics were also not modelled. Maximum joint torque limitations were not considered.

6.4 Control of Bipedal Gait

The algorithm used to control the bipedal robotic gait is based on Virtual Model Control [6].

6.4.1 Virtual Model Control

Virtual Model Control (VMC) is an abstract method to maintain the balance and lateral movement of a bipedal robot. Instead of using computed joint trajectories to achieve motion, the bipedal robot is attached to a virtual 'granny walker' which contains spring and damper components to specify the reaction forces at the ground required to maintain the altitude of the robot's centre of mass (CoM). The specified forces can then be used to calculate joint torques to indirectly control the balance of the bipedal robot. In the lateral direction, the model uses a virtual 'dogtrack bunny' maintain the robot's lateral motion of the CoM (see figure 6.4).

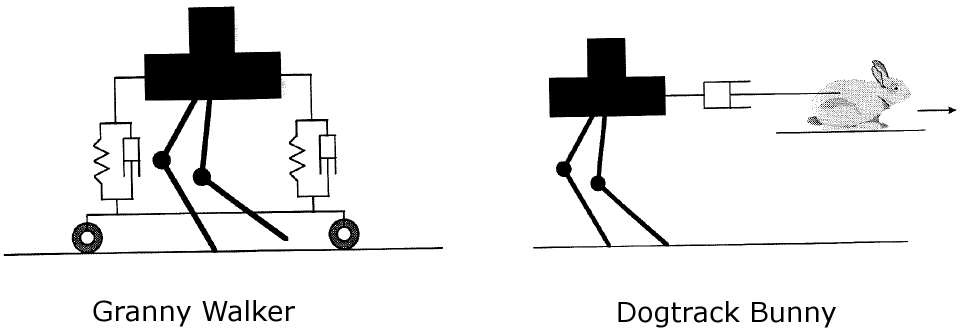

FIGURE 6.4: Virtual Model Control

The model effectively results in a P-D controller:

$$F_x = K_{px}(x_{desired} - x) + K_{dx}(\dot{x}_{desired} - \dot{x}) \tag{6.4}$$

$$F_y = K_{py}(y_{desired} - y) + K_{dy}(\dot{y}_{desired} - \dot{y}) \tag{6.5}$$

Where the inputs: $x_{desired}, y_{desired}$ are the desired positions of the CoM and $\dot{x}_{desired}, \dot{y}_{desired}$ are the desired velocity of the CoM.

And the outputs: F_x, F_y are the horizontal and vertical forces applied to the robot CoM respectively.

And the parameters: K_{px}, K_{py} are the proportional gains, K_{dx}, K_{dy} are the derivative gains,

6.4.2 Foot Force Distribution

VMC only specifies the total forces applied to the CoM of the entire robot assembly but since there are two feet a method is required to distribute these forces between the feet during the double-stance phase (when both feet are on the ground). A simple rule is to linearly distribute the force between the two feet according to the position of the CoM relative to the two feet. Variables w_F and w_R are the proportions of the robot's mass over each foot.

$$w_F = \begin{cases} 0 & \text{for } x_{CoM} < x_R \\ \frac{x_{CoM} - x_R}{x_F - x_R} & \text{for } x_R < x_{CoM} < x_F \\ 1.0 & \text{for } x_{CoM} > x_F \end{cases} \tag{6.6}$$

$$w_R = 1.0 - w_F \tag{6.7}$$

$$\begin{aligned} F_{yF} &= w_F F_y \\ F_{yR} &= w_R F_y \end{aligned} \tag{6.8}$$

where x_{CoM} is the absolute position of the CoM, x_F is the absolute position of the front foot and x_R is the absolute position of the rear foot (so x_F is always greater than x_R).

Distributing the lateral foot forces can be achieved by:

$$F_{xF} = \rho_F F_{yF} \tag{6.9}$$
$$F_{xR} = \rho_R F_{yR} \tag{6.10}$$

where ρ_F, ρ_R are the applied force ratios for each foot. These can usually be selected arbitrarily but as will be seen in section 6.5 may need to be constrained to prevent the bipedal robot from slipping. As a result F_{xF}, F_{xR} cannot be considered to be independent variables.

F_{yF}, F_{yR} can be solved for arbitrary values of $F_x, F_y, w_F, w_R, \rho_F$ and ρ_R:

$$F_x = F_{xF} + F_{xR} = \rho_F F_{yF} + \rho_R F_{yR} \tag{6.11}$$
$$F_y = F_{yF} + F_{yR} \tag{6.12}$$

$$F_{yF} = \frac{\rho_R F_y - w_R F_x}{w_F \rho_R - w_R \rho_F} \tag{6.13}$$
$$F_{yR} = \frac{\rho_F F_y - w_F F_x}{w_F \rho_R - w_R \rho_F} \tag{6.14}$$

For normal walking the applied force ratios (ρ_F, ρ_R) are chosen so that the vector of the force applied to the ground is directed from the contact point (the 'toe') to the robot's hip (see figure 6.5). This results in no moment occurring around the hip.

$$\rho_{F,normal} = tan(\theta_F) = \frac{x_{CoM} - x_F}{y_{CoM}} \tag{6.15}$$
$$\rho_{R,normal} = tan(\theta_R) = \frac{x_{CoM} - x_R}{y_{CoM}} \tag{6.16}$$

where y_{CoM} is the height of the CoM above the ground.

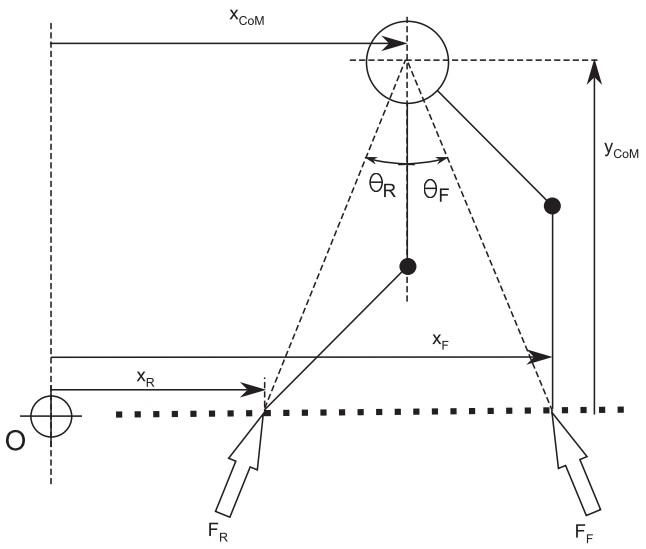

FIGURE 6.5: Applied Force Ratios

The above applies to the double-stance phase where both feet are in contact with the ground. The single-stance phase must be dealt with separately. The distribution of forces across a single foot is trivial and is given by:

$$F_{y,st} = F_y \tag{6.17}$$

$$F_{x,st} = \rho_{st} F_y \tag{6.18}$$

$$\rho_{st,normal} = \frac{F_x}{F_y} \tag{6.19}$$

The swing leg torques (τ_{sw}) are specified by an operation space controller (see section 6.4.3).

The final joint torques can be determined depending on which stance phase the robot is operating in:

$$\tau_i = \begin{bmatrix} \mathbf{0}_{2\times 1} \\ \tau_1 \\ \tau_2 \end{bmatrix} \tag{6.20}$$

Where in the double stance phase:

$$\tau_1 = -J_1^T F_F \tag{6.21}$$

$$\tau_2 = -J_2^T F_R \tag{6.22}$$

if $x_1 > x_2$, or:

$$\tau_1 = -J_1^T F_R \tag{6.23}$$
$$\tau_2 = -J_2^T F_F \tag{6.24}$$

if $x_1 < x_2$.

And in the single stance phase:

$$\tau_1 = -J_1^T F_{st} \tag{6.25}$$
$$\tau_2 = \tau_{sw} \tag{6.26}$$

if Foot 1 is in contact with the ground, or:

$$\tau_1 = \tau_{sw} \tag{6.27}$$
$$\tau_2 = -J_2^T F_{st} \tag{6.28}$$

if Foot 2 is in contact with the ground.

Note the negative sign when the foot is in contact with the ground. This is because the forces are applied *to* the ground.

6.4.3 Step Control and Foot Placement

The final element in bipedal walking is choosing when to take a step, selecting the desired location of the swing foot during the single-stance phase and the controller to move the swing leg.

The decision to take a step was decided to be when the CoM was vertically over a foot. After this point the robot can not easily arrest its motion (since it does not include ankles) and so taking a step is necessary. A second trigger is when either leg becomes completely straight ($q_3 = 0$ or $q_5 = 0$) because in this case the CoM cannot continue to move without causing the foot of the straight leg to drag.

The target foot position was tuned to maintain a nominal stride length $D_{s,nom}$ for a given robot velocity $\dot{x}_{nom}$. This stride length was adjusted proportionately to the velocity, decreasing the stride length at lower velocities and increasing it at higher velocities. This

improved the overall stability of the bipedal robot gait. The equation for calculating the stride length d_s is:

$$d_s = D_{s,nom} + K_{stride}(\dot{x} - \dot{x}_{nom}) \tag{6.29}$$

where K_{stride} is the velocity-adjustment gain and $\dot{x}$ is the current velocity of the bipedal robot CoM.

The control of the swing leg was achieved by specifying a sinusoidal trajectory from the takeoff point to the landing point, with the maximum height of the foot vertically below the CoM. The leg was controlled using position-feedback operational space control [60].

6.4.4 Slip Response

No additional response was developed to compensate for the destabilising effects of slip. It is intended that the friction estimator and slip prevention algorithm (section 6.5) will be sufficient to prevent slip from occurring at all.

6.5 Friction Estimator and Slip Prevention

The non-slip friction estimator was implemented as described in section 4.6: each time-step the contact forces were measured and the lateral velocity of the foot was determined through forward-kinematics. The RLS algorithm was applied and estimate of the friction constraint was updated.

The estimator treats each step as being onto a potential new, unknown surface as so makes no assumption about the coefficient of friction. To this end, the estimator was applied to each foot independently and each time the foot left the ground the estimator was reinitialised to 0 and the convergence flag cleared. To handle cases when the two feet were on different surfaces, such as when transferring to a new surface or stepping on a slippery patch, the applied force ratio ρ was separated into ρ_F and ρ_R.

The bipedal robot controller compensates for the the coefficient of friction by updating its internal value (the 'controller value') of μ_c when the convergence flag a is set and holding that value until the estimator is reset. To help ensure stability by compensating for an inaccurate measurement, the slip prevention controller value was also multiplied by a safety factor K_{safety}. To prevent slip from occurring the applied force ratio ρ_i must be no greater than the coefficient of friction. This results in an equation for ρ_i:

$$\rho_i = \begin{cases} -\mu_c & \text{if } \rho_{i,normal} < -\mu_c \\ \mu_c & \text{if } \rho_{i,normal} > \mu_c \\ \rho_{i,normal} & \text{otherwise} \end{cases} \tag{6.30}$$

where $\rho_i = \rho_F, \rho_R$ (in double-stance phase) or $\rho_i = \rho_{st}$ (in single-stance phase) and μ_c is the coefficient of friction between the robot's foot and ground surface.

If ρ_i is less than $\rho_{i,normal}$ (which will occur when $|\rho_{i,normal}| > \mu_c$) then the desired lateral acceleration may not be achieved. This is acceptable since it is more important that the robot maintains balance and does not slip, rather than that it achieves its desired lateral acceleration.

6.6 Summary

This chapter presented the equations of motion for a 6-DoF bipedal robot, ground impact, friction model and a simple walking algorithm. The walking algorithm was augmented with the estimator from chapter 4 and a slip prevention algorithm was implemented.

Chapter 7 presents the results of the bipedal robot walking on two surfaces both with and without the slip prevention algorithm.

Chapter 7

Simulation Results

In this chapter, the bipedal robot gait simulation as presented in chapter 6 was performed to investigate the effects of implementing the non-slip friction estimation algorithm outlined chapter 4 and the ability for the robot to dynamically adjust to surfaces of varying and unknown coefficients of friction. This is achieved by simulating the bipedal robot stepping onto a low-friction surface both with and without the friction estimation algorithm. The availability of an estimate of the coefficient of friction allows for the use of the slip-prevention algorithm outlined in section 6.5. The results of the simulation without friction estimation are presented in section 7.2, the results of the simulation with friction estimation are presented in section 7.3. The comparison of the performance, highlighting the efficacy of the proposed estimator, is presented in section 7.4.

It should be noted that the bipedal robot has no prior knowledge of the surface friction conditions and makes no assumption about future conditions.

7.1 System Parameters

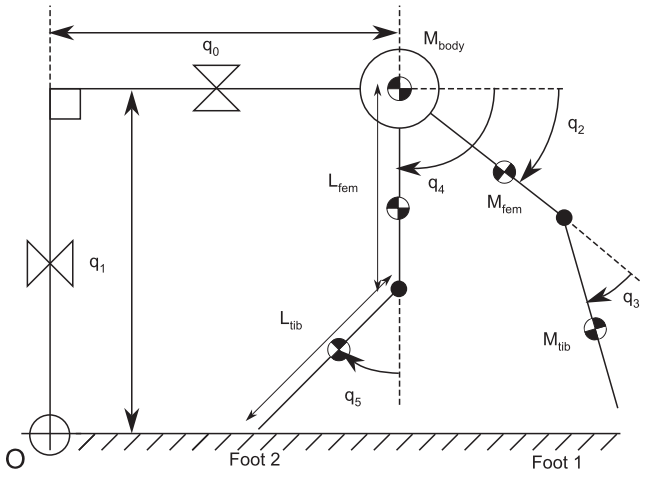

FIGURE 7.1: Model of Bipedal Robot

In all the simulations the following model parameters were used (see figure 6.1):

- Mass of Body: $M_{body} = 3.0kg$
- Mass of Femurs (Links 2 and 4): $M_{fem} = 0.1kg$
- Length of Femurs: $L_{fem} = 0.5m$
- Moment of Inertia of Femurs: $I_{tib} = 0.1kgm^2$
- Mass of Tibias (Links 3 and 5): $M_{tib} = 0.1kg$
- Length of Tibias: $L_{tib} = 0.5m$
- Moment of Inertia of Tibias: $I_{tib} = 0.1kgm^2$

The ground impact parameters are:

- $k = 50000$
- $b = 35000$
- $n = p = q = 1.0$

The control parameters are:

- $\dot{x}_{desired} = 0.5\text{m/s}$

- $K_{dx} = 50$
- $y_{desired} = 0.96\text{m}$
- $\dot{y}_{desired} = 0\text{m/s}$
- $K_{py} = 130$
- $K_{dy} = 50$
- Nominal Stride Length: $D_{s,nom} = 0.5\text{m}$
- Stride Gain: $K_{stride} = 0.3$

And the estimator parameters are:

- Forget factor: $\lambda = 0.99$
- Error Threshold: $\epsilon = 230$
- Error Horizon: $N = 20$
- Slip Prevention Safety gain: $K_{safety} = 0.90$

The surface friction parameters are:

- 'High' friction surface: $\mu_c = 1.0$
- 'Low' friction surface: $\mu_c = 0.4$
- Surface transition position = 2.25m
- $s_p = 0.001$

The estimator and control algorithm was run with a servo-time of 0.001s (1000Hz).

7.2 Transition From High to Low Friction Surface without Slip Prevention

The following simulation was performed without friction estimation or slip prevention.

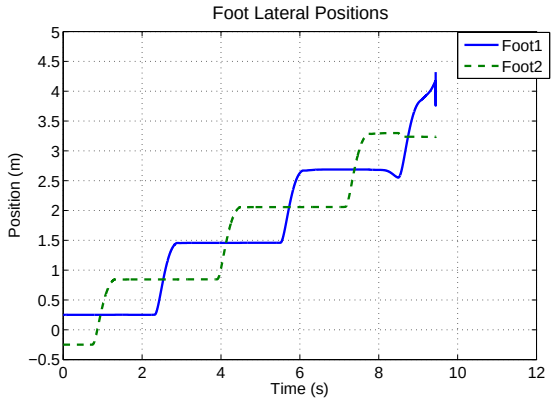

(a) Foot Positions

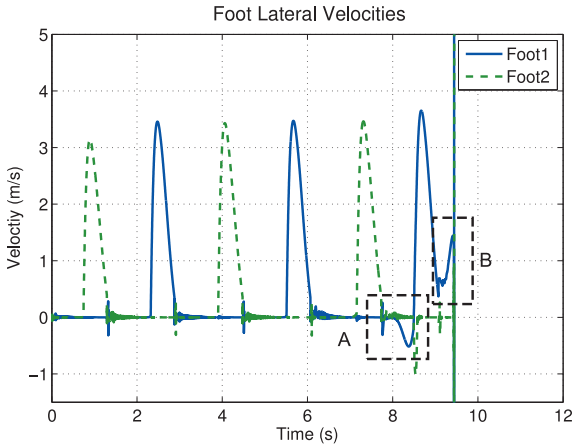

(b) Foot Velocities

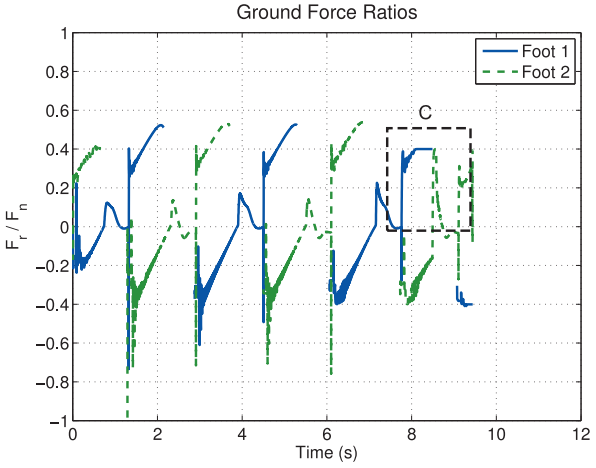

(c) Ground Reaction Force Ratios

FIGURE 7.2: Results of Simulation without Slip Prevention

Figure 7.2(a) shows the foot positions in the x direction during the simulation. Foot

1 starts with an initial position of +0.5m and Foot 2 starts with an initial position of -0.5m. At $t = 0.75s$ the robot takes its first step, lifting Foot 2 of the ground and placing it at $x_2 = 0.85m$ at $t = 1.3s$. The surface transition occurs at $x = 2.25m$ thus Foot 1 contacts the new surface at $t = 6.1s$ and Foot 2 contacts the new surface at $t = 7.8s$. It can be seen at $t = 8.2s$ that Foot 1 slips backwards, shortly before Foot 2 at $t = 8.5s$ (see Fig 7.3). It should be noted that the simulation was supposed to be run for a total of 12 seconds but at $t = 9.4s$ it fails numerically due to the slip causing a variable to increase to infinity. After $t = 9.4s$ the robot can be said to have failed. In reality this failure would be equivalent to a physical robot or bipedal creature slipping and falling.

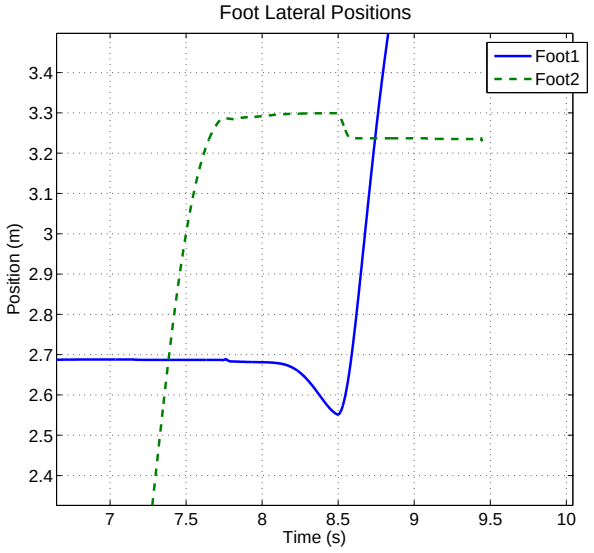

FIGURE 7.3: Foot Positions (zoomed in view of Fig 7.2(a))

Figure 7.2(b) shows the foot velocities in the x direction. The first step of Foot 2 can be seen as a sudden increase in velocity at $t = 0.75s$ before coming to a halt at $t = 1.3s$. The oscillations at each foot landing is due to the spring-damper impact model. The slip phenomenon at $t = 8.2s$ is shown by a sudden negative velocity at Foot 1 (see region A: Fig 7.4) and is only arrested because the robot lifts the foot in order to step. The transition to the single-stance phase at $t = 8.5s$ (when Foot 1 reaches positive velocity) coincides with the slip of Foot 2. Finally at $t = 9.1s$ the positive velocity of Foot 1 is not arrested by contact with the ground and instead slips significantly, the velocity increasing to infinity at $t = 9.4s$ (see region B).

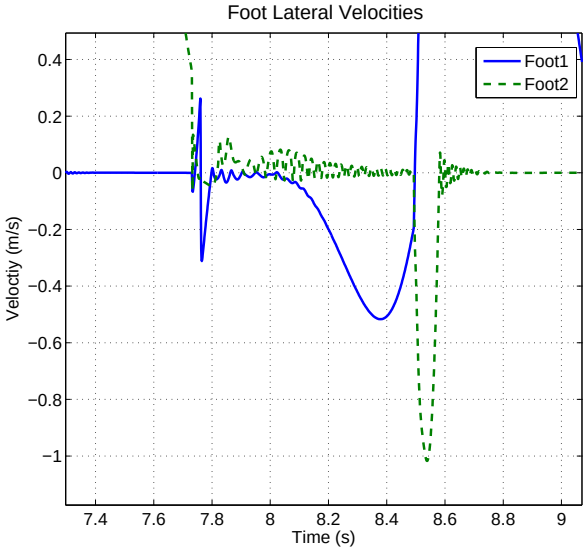

FIGURE 7.4: Foot Velocities (zoomed in region A of Fig 7.2(b))

Figure 7.2(c) shows the ratios of the friction contact force to the normal contact force (F_r/F_n) during the bipedal robot walk cycle. Note that for the first surface ($x < 2.25m$: $t < 6.1s$ for Foot 1, $t < 7.8s$ for Foot 2) $\mu = 1.0$ and for the second surface ($x > 2.25m$) $\mu = 0.4$. From the initial stance, the force ratio at Foot 1 (u_1) decreases in magnitude (θ_1 gets smaller in Fig 6.5) and the force ratio at Foot 2 (u_2) increases in magnitude (θ_2 gets larger) as the CoM moves in the positive x direction towards Foot 1. At $t = 0.75$ Foot 2 lifts from the ground causing u_2 to go to infinity (since F_{n2} goes to zero) and the bipedal robot to go into the single-stance phase.

The first single-stance phase begins at $t = 0.75s$ and ends when Foot 2 impacts the ground at $t = 1.3s$ (the large oscillations are due to the spring-damper impact model). The cycle of double-stance to single-stance phase-transitions repeats. From figure 7.2(a) it can be seen that Foot 1 impacts the new low-friction surface at $t = 6.1s$ and slips at $t = 8.2s$. This slip can be clearly seen by the saturation of u_1 from $t = 8.5s$ to when Foot 1 is lifted at $t = 8.5s$ (see region C: Fig 7.5). The final single-stance phase lasts until Foot 1 impacts the ground at $t = 9.1$ where the value of u_1 saturates to 0.4 instantly causing the foot to slip and the simulation to fail.

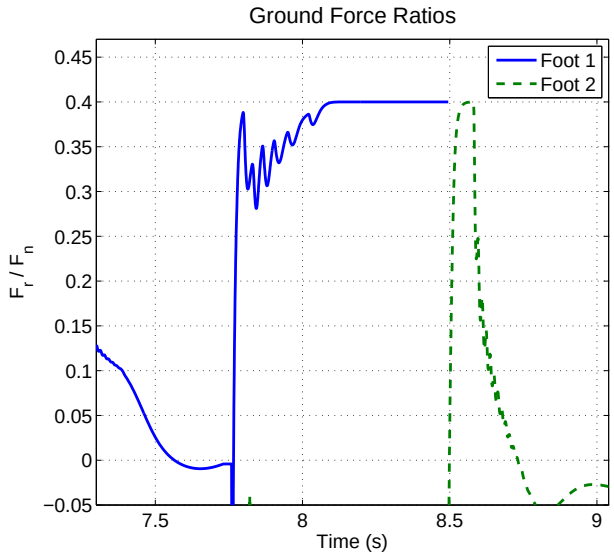

FIGURE 7.5: Ground Reaction Force Ratios (zoomed in region C of Fig 7.2(c))

7.3 Transition From High to Low Friction Surface with Slip Prevention

Section 7.2 showed the results of the bipedal robot walking without the slip prevention algorithm (see section 6.5). This section will look at the results of the bipedal robot walking with the slip prevention algorithm.

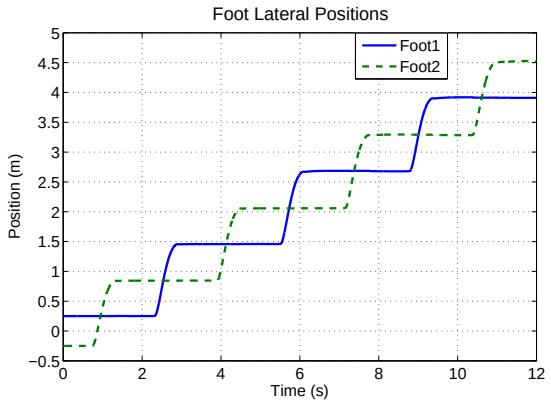

(a) Foot Positions

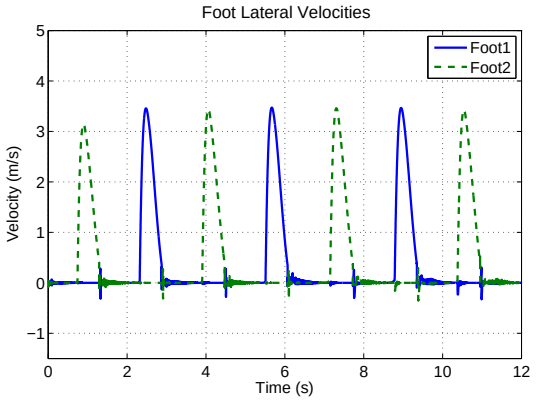

(b) Foot Velocities

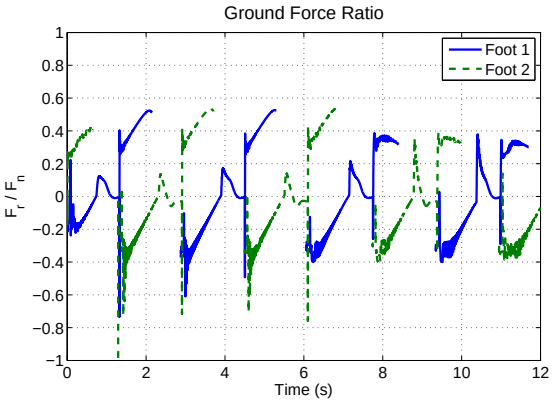

(c) Ground Reaction Force Ratios

FIGURE 7.6: Results of Simulation with Slip Prevention

As in section 7.2, figure 7.6(a) shows the lateral foot positions of the bipedal robot. Prior to $t = 6.1s$ Foot 1 performs the same as per without slip prevention as is the same with Foot 2 prior to $t = 7.8s$. After the feet contact the new surface the robot maintains its stable walking pattern, the feet following roughly the same pattern as on

the high-friction surface but with no slip occurring (see Fig 7.7). The simulation is able to progress through the intended 12 seconds.

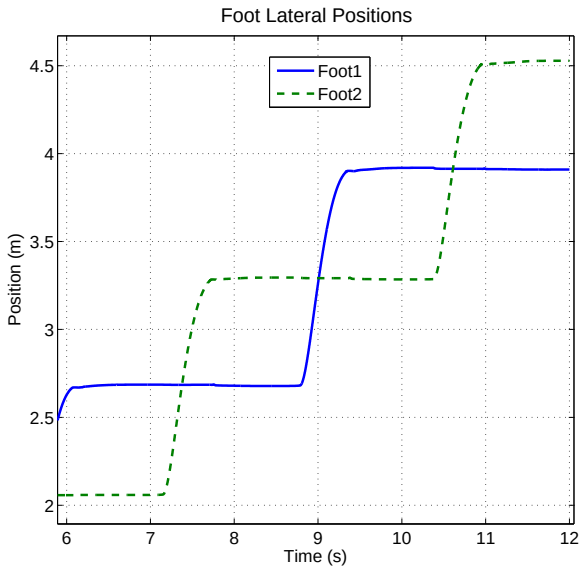

FIGURE 7.7: Foot Positions (zoomed in view of Fig 7.6(a))

Figure 7.6(b) shows the lateral foot velocities. With the exception of the oscillations caused by the impact model, there is no significant negative velocity that would indicate a foot slipping and the velocity profile is unchanged between the two different surfaces on which the bipedal robot walks.

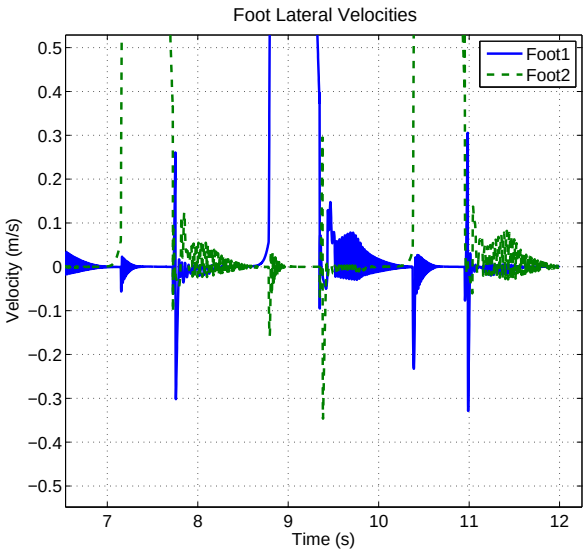

FIGURE 7.8: Foot Velocities (zoomed in view of Fig 7.6(b))

Figure 7.6(c) shows the ratios of the friction contact force to the normal contact force (F_r/F_n) during the bipedal walk cycle with slip prevention.

On the high-friction surface ($\mu = 1.0$) the it is identical to the behaviour without slip prevention. Since the applied ratio never gets close to the friction limit even in the uncompensated case, no slip prevention is required and so the behaviour is unaffected.

On the low-friction surface ($\mu = 0.4$) there is a noticeable change. In the high-friction surface the force ratio of the rear leg (leg with F_r/F_n ¿ 0) increases linearly until the foot is lifted, however in the low-friction case the force ratio increases but then holds at a constant value below the coefficient of friction (see Fig 7.9) before lifting off the ground. The slip prevention successfully prevents the force ratio from saturating and thus no slip occurs.

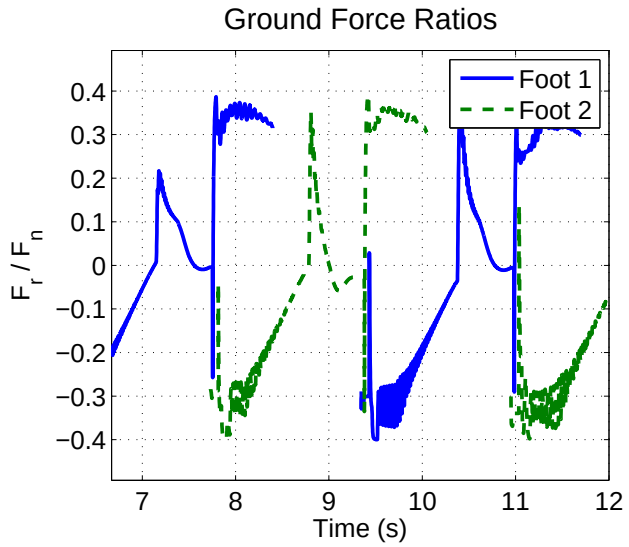

FIGURE 7.9: Ground Reaction Force Ratios (zoomed in view of Fig 7.6(c))

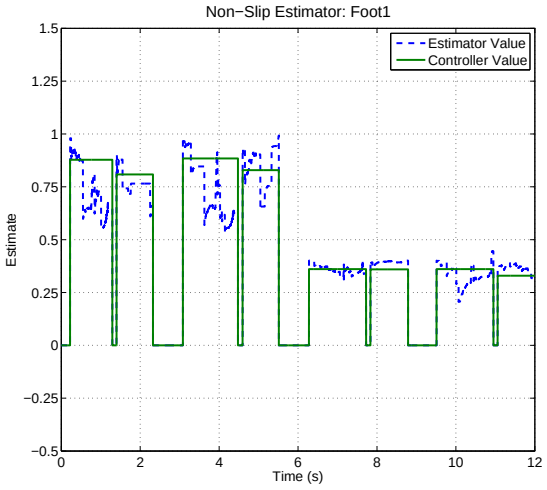

(a) Foot 1

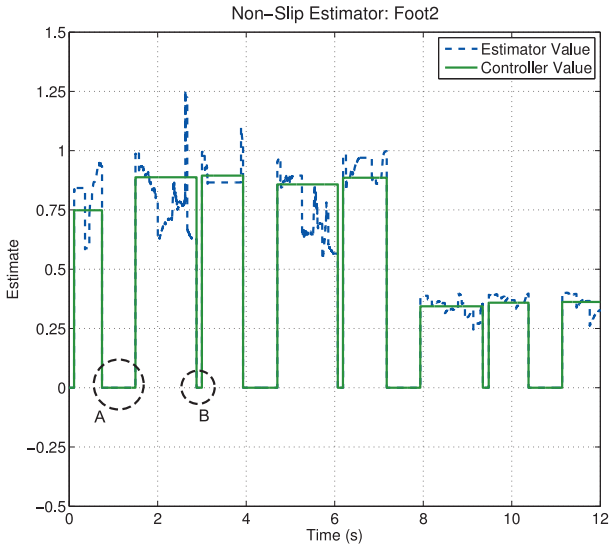

(b) Foot 2

FIGURE 7.10: Friction Estimator

Figure 7.10 shows the behaviour of the non-slip friction estimator during the gait cycle for each foot. The Estimator Value is the current value of the estimator whereas the Controller Value is the value used by the controller to prevent slip from occurring. (see section 6.5). For clarity the estimator value is only plotted when the convergence flag is 1 and is set to 0 when the convergence flag is zero. For each step the estimator converges to a value approximately 0.1s after impact occurs. The estimator is reset each time the foot leaves the ground (region A). The short times where the estimator is reset whilst the foot is on the ground (region B) is due to the impact of the other landing foot causing

the stance leg to momentarily leave the ground due to the reverberation from using a continuous ground impact model.

As the robot steps on the high-friction surface the estimator converges to a value of approximately 1.0, thus the controller value reaches a value of 0.9 (1.0 * K_{safety}). As in figure 7.6(c) this is well above the value that the ground force ratio reaches and so no slip prevention is applied.

When Foot 1 contacts the new surface the estimator quickly converges to the new coefficient of friction of 0.4 and the slip prevention controller thus reaches a value of about 0.36 (see Fig 7.11). This is the value at which the ground force ratio holds constant in fig 7.9 and is due to the active slip prevention. Thanks to the slip prevention algorithm, at no point during this simulation does the bipedal robot slip.

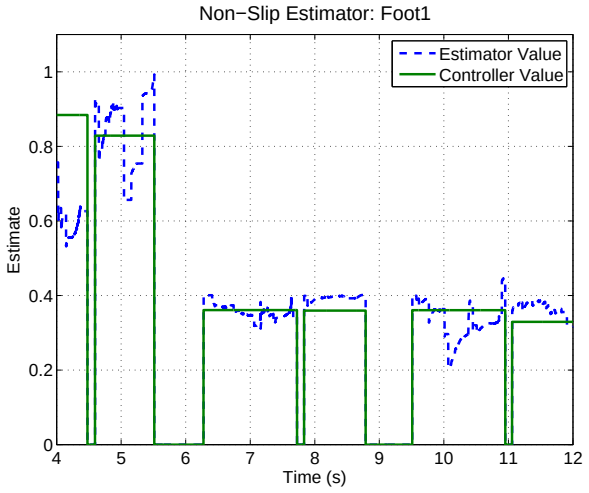

FIGURE 7.11: Friction Estimator: Foot 1 (zoomed in view of Fig 7.10(a))

In Fig 7.10 there still exists some fluctuation in the estimated value of the coefficient of friction. This will be separated into two regions for explanation.

During the region of coefficient of friction = 1.0: In this region, the applied force ratio only achieves a value of approx 0.5 before the foot is lifted. Since the applied force ratio stays much lower than the coefficient of friction, the tangential foot velocity remains small. There is also some noise in the simulation due to the use of a stiff friction model combined with a non-stiff solver (ode45). The signal-to-noise ratio is too low for the algorithm to accurately estimate the coefficient of friction. The foot leaves the ground before the applied force ratio becomes large enough for an accurate estimate. This is acceptable as the applied force ratio is never at risk of exceeding the coefficient of friction.

During the region of coefficient of friction = 0.4: This region shows how the estimator behaves when the applied force ratio is at risk of exceeding the coefficient of friction. Although there is some oscillation in the estimated value, it is small and oscillates around approximately the correct value of the coefficient of friction. The estimator works because the signal-to-noise ratio is higher than in the previous region. This fluctuation shows that the estimator is not perfectly robust to noise.

7.4 Comparing the Effect of Slip Prevention

This section will look closer at the difference in the behaviour of the bipedal robot both with and without the slip prevention algorithm. Corresponding results from sections 7.2 and 7.3 are compared in the following plots, representing the results of the systems with and without slip prevention.

For the clarity of presentation only the states and parameters associated with Foot 1, for both the cases of with and without the slip prevention algorithm will be shown.

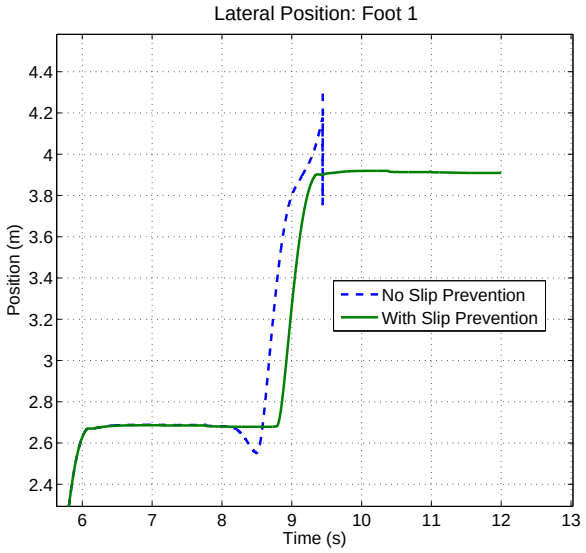

FIGURE 7.12: Foot Position

Figure 7.12 shows the difference in foot positions between the two cases. Prior to $t = 8.1s$ the results are the same, after which the the foot slides backwards in the no-prevention case but maintains its position in the slip prevention case. The foot also leaves the ground earlier because the backwards slip causes the leg to extend, triggering the step response. At the next impact the no-prevention case slips in the positive direction causing the simulation to fail whereas in the slip prevention case the foot successfully lands without slipping and the bipedal robot continues to walk for the entire 12 seconds.

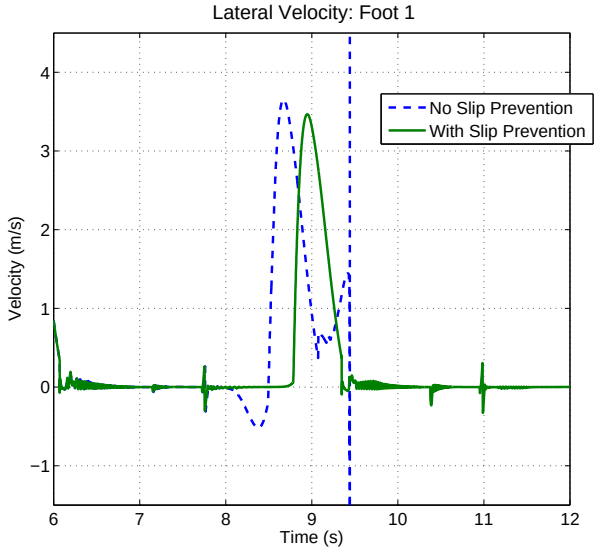

FIGURE 7.13: Foot Velocity

Figure 7.13 shows the difference in foot velocities between the two cases. At $t = 8.1s$ the velocity of the foot in the no-prevention case increases in the negative x direction whereas the velocity of the foot in the slip prevention case is maintained at zero. As seen in figure 7.12 in the no-prevention case the foot velocity increases as the foot is lifted off the ground and moved to the new step position at but is not arrested by contact with the surface and increases to infinity. In the slip prevention case however the foot is arrested on impact and maintains a velocity of zero.

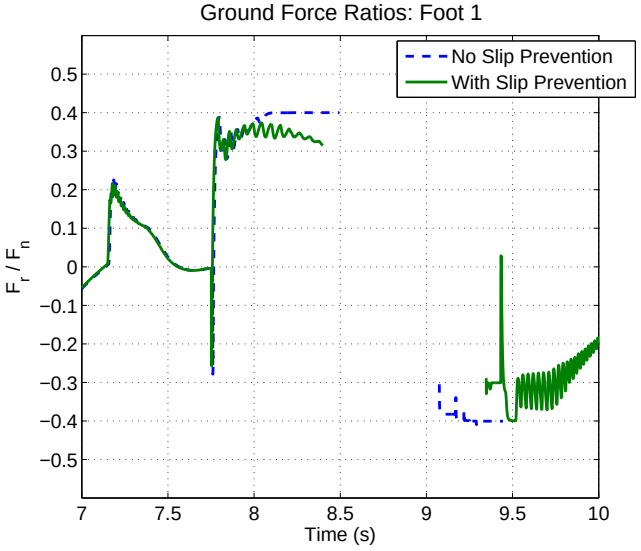

FIGURE 7.14: Ground Force Ratios

Figure 7.14 shows the difference in ground force ratios between the two cases. Prior to $t = 8.1s$ the two curves coincide but at $t = 8.1s$ the force ratio in the no-prevention case saturates at the value of the coefficient of friction of the low-friction surface ($\mu_c = 0.4$) until the foot is lifted. The empty space from $t = 8.5s$ to $t = 9.1s$ is due to the foot not being in contact with the ground.

In the slip prevention case the force ratio maintains a constant value (approx.= 3.6) just below the value of the coefficient of friction and does not saturate due to the slip prevention algorithm. At $t = 9.1$, in the no-prevention case, the foot impacts the ground and instantly saturates quickly leaded to the simulation failing at $t = 9.4s$. In the slip prevention case however the contact force ratio does not saturate after impact at $t = 9.5s$ and continues to the end of the simulation.

7.5 Conclusion

This chapter presented a simulation of a bipedal robot walking from a surface of high-friction onto a surface of low-friction both with and without a slip prevention algorithm.

It was demonstrated that without a slip prevention algorithm the robot was unable to walk on the low-friction surface due to the ground reaction force saturating, thus failing the arrest the slip velocity of the feet and causing the simulation to fail.

With a slip-prevention algorithm however, the robot was able to step and maintain balance on the low-friction surface without slipping and was able to continue until the end of the simulation.

Chapter 8

Conclusions

This thesis proposed an estimator-based solution to the problem of determining the coefficient of friction between the ground surface and the foot of a bipedal robot without slipping.

Requirements for a successful estimator were developed including requirements of the model as well as an appropriate regression technique. Several models of contact friction were investigated and one was chosen to be the basis of the model-based estimator based on the proposed requirements. The Recursive Least Squares regression technique was used to estimate the model parameters in an online environment and the regression model was developed from the chosen friction model. An algorithm to determine when the estimate was sufficiently close to its final value to be useful was also designed.

The estimator was experimentally validated using a simple drag test rig using three contacting surfaces of varying coefficient of friction. These different coefficients of friction were achieved by changing the two surfaces in contact. Since one surface was constrained by the experimental apparatus used to measure the contact forces, the coefficient of friction was varied by changing the material affixed to the drag rig. The three coefficients of friction were approximately 1.0, 1.25 and 0.7. The estimator was successful in estimating the coefficient of friction before slip occurred in all tests. The convergence-detection algorithm was successful in determining when convergence had been satisfactorily reached.

A 6-link bipedal robot with a floating base was modelled along with ground impact and friction models. A Virtual Model Control based controller was developed with stepping control to allow the bipedal robot to balance and walk on a flat surface. The controller was adapted with a slip prevention algorithm so that it could successfully operate on a surface with an arbitrary coefficient of friction (if known or estimated). The system was

simulated on a in-house simulator based on the Dormand-Prince ordinary differential equation solver.

The estimator was implemented in the bipedal gait controller for each foot independently and tested on a variety of surface conditions. The slip prevention algorithm was shown to be able to successfully allow a bipedal robot to walk on a surface with coefficient of friction of 0.4 without prior knowledge of the value and without slipping whereas without the slip-prevention algorithm it was unable to.

Chapter 9

Future Work

In this thesis an estimator to solve the problem of determining the coefficient of friction between the ground surface and the foot of a bipedal robot was successfully developed and tested. However there are several areas in which the technique can be advanced.

9.1 Friction Oriented Biped Controller

The controller outlined in chapter 6 was a simple, intuitive algorithm that operated on hand-tuned control gains and walking parameters with friction compensation added on. Knowledge of the coefficient of friction however would allow a high-level controller to dynamically adjust operating parameters in order to optimise the bipedal robot's stability, balance, speed, safety and energy efficiency for any given surface.

9.2 Friction Models and Estimation Techniques

The estimator developed in this thesis is admittedly a simple one based on a first-order friction model and linear regression algorithm. A second-order Bliman-Sorine friction model was investigated in section 4.2 but was found to be unsuitable for use with a least squares estimator. Investigation into more complex, non-linear friction models may result in a faster and more accurate estimate of the coefficient of friction. Advanced estimation techniques such as sliding-mode estimation or non-linear estimators could also be used to improve performance when combined with advanced friction models. Finally the estimator was implemented with single sensors for each variable and little signal conditioning. Better data could be obtained using Kalman filtering along with extra sensors on the robot.

9.3 Implementation in a Physical Robot

The next step in development would be to implement the estimator in a physical bipedal root and evaluate both the performance of the estimator as well as the robot's ability to balance, walk and compensate for low-friction surfaces in a physical environment. This would require investigation into the sensors required for the successful performance of the estimator. Issues such as accuracy of measurements of tangential velocity and ground reaction forces, sensitivity to noise and disturbances, and the rate at which data is acquired all will need to be investigated.

9.4 Sloped Surfaces and Deformable Surfaces

The primary motivation for the work in this thesis was to improve the ability of a bipedal robot to operate in highly variable, human-like environments. There are two other major environments to which the estimator could be extended.

The first is the problem of deformable terrain such as sand, soil, snow, mud etc. On these surfaces it is unknown as to how well the estimator will perform, or whether it performs at all. Investigation into the dynamics of deformable terrains will help determine whether a single model can be used or if multiple models with switching conditions are required. This approach could improve the stability and performance of bipedal robots on soft surfaces.

The second is the problem of sloped and rugged surfaces. So far the estimator has only been utilised on surfaces that are known to be flat. The problem of bipedal robots walking on sloped surfaces has been investigated by others with many different approaches such as passivity based [61] where the slope is not determined but simply compensated for and in-sole sensors to measure the slope [62] and other surface conditions [63] directly. The friction estimator would have to be combined with the slope information in order to determine the normal contact force, the tangential (friction) force and the tangential foot velocity.

Bibliography

[1] M. Vukobratovic and D. Juricic, "Contribution to the synthesis of biped gait," *IEEE Transactions on Biomedical Engineering*, vol. 16, pp. 1–6, 1969.

[2] "History of the humanoids: E0 - http://world.honda.com/asimo/history/e0.html."

[3] M. Zarrugh and C. Radcliffe, "Computer generation of human gait kinematics," *Journal of biomechanics*, vol. 12, no. 2, pp. 99–111, 1979.

[4] H. Miura and I. Shimoyama, "Dynamic walk of a biped," *The International Journal of Robotics Research*, vol. 3, no. 2, p. 60, 1984.

[5] S. Kajita, F. Kanehiro, K. Kaneko, K. Fujiwara, K. Harada, K. Yokoi, and H. Hirukawa, "Biped walking pattern generation by using preview control of zero-moment point," in *International Conference on Robotics and Automation*, vol. 2. IEEE, 2003, pp. 1620–1626.

[6] J. Pratt, C. Chew, A. Torres, P. Dilworth, and G. Pratt, "Virtual model control: An intuitive approach for bipedal locomotion," *The International Journal of Robotics Research*, vol. 20, no. 2, pp. 129–143, 2001.

[7] J. Park, "Fuzzy-logic zero-moment-point trajectory generation for reduced trunk motions of biped robots," *Fuzzy sets and systems*, vol. 134, no. 1, pp. 189–203, 2003.

[8] W. Miller III, "Real-time neural network control of a biped walking robot," *Control Systems Magazine*, vol. 14, no. 1, pp. 41–48, 1994.

[9] K. Hirai, M. Hirose, Y. Haikawa, and T. Takenaka, "The development of honda humanoid robot," in *Robotics and Automation, 1998. Proceedings. 1998 IEEE International Conference on*, vol. 2. IEEE, 1998, pp. 1321–1326.

[10] K. Kaneko, F. Kanehiro, S. Kajita, K. Yokoyama, K. Akachi, T. Kawasaki, S. Ota, and T. Isozumi, "Design of prototype humanoid robotics platform for hrp," in *Intelligent Robots and Systems, 2002. IEEE/RSJ International Conference on*, vol. 3. IEEE, 2002, pp. 2431–2436.

[11] J. Chestnutt, J. Kuffner, K. Nishiwaki, and S. Kagami, "Planning biped navigation strategies in complex environments," in *IEEE Int. Conf. Hum. Rob., Munich, Germany*. Citeseer, 2003.

[12] S. Collins and A. Ruina, "A bipedal walking robot with efficient and human-like gait," in *Robotics and Automation, 2005. ICRA 2005. Proceedings of the 2005 IEEE International Conference on*. IEEE, 2005, pp. 1983–1988.

[13] Y. Zheng, "Acceleration compensation for biped robots to reject external disturbances," *Systems, Man and Cybernetics, IEEE Transactions on*, vol. 19, no. 1, pp. 74–84, 1989.

[14] Y. Zheng, J. Shen, and F. Sias Jr, "A motion control scheme for a biped robot to climb sloping surfaces," in *Robotics and Automation, 1988. Proceedings., 1988 IEEE International Conference on*. IEEE, 1988, pp. 814–816.

[15] H. Kang, K. Hashimoto, H. Kondo, K. Hattori, K. Nishikawa, Y. Hama, H. Lim, A. Takanishi, K. Suga, and K. Kato, "Realization of biped walking on uneven terrain by new foot mechanism capable of detecting ground surface," in *Robotics and Automation (ICRA), 2010 IEEE International Conference on*. IEEE, 2010, pp. 5167–5172.

[16] J. H. Park and O. Kwon, "Reflex control of biped robot locomotion on a slippery surface," *Proc. IEEE Int. Conference on Robotics and Automation*, pp. 4134–4139, 2001.

[17] H. Yamamoto and K. Ohnishi, "An approach to stable walking on unknown slippery floor for biped robot," *Annual Conference of the IEEE Industrial Electronics Society*, pp. 1728–1733, 2001.

[18] K. Kaneko, F. Kanehiro, S. Kajita, K. Fujiwara, and K. Harada, "Slip observer for walking on a low friction floor," *Proceedings of 2004 IEEE/RSJ International Conference on Intelligent Robots and Systems*, pp. 3546–3552, 2004.

[19] J. Yamaguchi, A. Takanishi, and I. Kato, "Development of a biped walking robot adapting to a horizontally uneven surface," in *Intelligent Robots and Systems' 94.'Advanced Robotic Systems and the Real World', IROS'94. Proceedings of the IEEE/RSJ/GI International Conference on*, vol. 2. IEEE, 1994, pp. 1156–1163.

[20] H. Hirukawa, "Walking biped humanoids that perform manual labour," *Philosophical Transactions of the Royal Society A: Mathematical, Physical and Engineering Sciences*, vol. 365, no. 1850, p. 65, 2007.

[21] T. Nishiyama, H. Hoshino, K. Sawada, A. Baba, T. Sekine, W. Yamada, A. Terasawa, R. Nakajima, Y. Tokunaga, and M. Yoneda, "Communication agent embedded in humanoid robot," in *SICE 2003 Annual Conference*, vol. 2. IEEE, 2003, pp. 1514–1519.

[22] F. Hardarson, "Locomotion for difficult terrain," *Dept. Mach. Des., Royal Inst. Technol., Stockholm, Sweden, Tech. Rep. TRITA-MMK*, vol. 3, pp. 1400–1179, 1998.

[23] M. Raibert and E. Tello, "Legged robots that balance," *IEEE Expert*, vol. 1, no. 4, pp. 89–89, 1986.

[24] D. Wright and W. Chun, "Advanced rover for planetary exploration," *Mobile robots III*, pp. 120–127, 1989.

[25] Z. Wang and H. Gu, "A review of locomotion mechanisms of urban search and rescue robot," *Industrial Robot: An International Journal*, vol. 34, no. 5, pp. 400–411, 2007.

[26] A. Bejczy, "Towards development of robotic aid for rehabilitation of locomotion-impaired subjects," in *Proceedings of the First Workshop on Robot Motion and Control: RoMoCo'99: June 28-29, 1999, Kiekrz, Poland.* IEEE, 1999, p. 9.

[27] Y. Sugahara, K. Hashimoto, H. Sunazuka, M. Kawase, A. Ohta, C. Tanaka, H. Lim, and A. Takanishi, "Towards the biped walking wheelchair," in *Biomedical Robotics and Biomechatronics, 2006. BioRob 2006. The First IEEE/RAS-EMBS International Conference on.* IEEE, 2006, pp. 781–786.

[28] C. Yang and Q. Wu, "Effects of gravity and friction constraints on bipedal balance control," in *Control Applications, 2005. CCA 2005. Proceedings of 2005 IEEE Conference on.* IEEE, 2005, pp. 1093–1098.

[29] B. Stephens and C. Atkeson, "Modeling and control of periodic humanoid balance using the linear biped model," in *International Conference on Humanoid Robots.* IEEE, 2009, pp. 379–384.

[30] L. Strandberg, "On accident analysis and slip-resistance measurement," *Ergonomics*, vol. 26, no. 1, pp. 11–32, 1983.

[31] M. Redfern and B. Bidanda, "Slip resistance of the shoe-floor interface under biomechanically-relevant conditions," *Ergonomics*, vol. 37, no. 3, pp. 511–524, 1994.

[32] J. Hanson, M. Redfern, and M. Mazumdar, "Predicting slips and falls considering required and available friction," *Ergonomics*, vol. 42, no. 12, pp. 1619–1633, 1999.

[33] X. Mu and Q. Wu, "Development of a complete dynamic model of a planar five-link biped and sliding mode control of its locomotion during the double support phase," *International Journal of Control*, vol. 77, no. 8, pp. 789–799, 2004.

[34] S. Setiawan, J. Yamaguchi, S. Hyon, and A. Takanishi, "Physical interaction between human and a bipedal humanoid robot-realization of human-follow walking," in *Robotics and Automation, 1999. Proceedings. 1999 IEEE International Conference on*, vol. 1. IEEE, 1999, pp. 361–367.

[35] J. Kim, I. Park, J. Lee, M. Kim, B. Cho, and J. Oh, "System design and dynamic walking of humanoid robot khr-2," in *Robotics and Automation, 2005. ICRA 2005. Proceedings of the 2005 IEEE International Conference on*. IEEE, 2005, pp. 1431–1436.

[36] K. Nishiwaki, S. Kagami, Y. Kuniyoshi, M. Inaba, and H. Inoue, "Online generation of humanoid walking motion based on a fast generation method of motion pattern that follows desired zmp," in *Intelligent Robots and Systems, 2002. IEEE/RSJ International Conference on*, vol. 3. IEEE, 2002, pp. 2684–2689.

[37] P. Wieber, "Viability and predictive control for safe locomotion," in *Intelligent Robots and Systems, 2008. IROS 2008. IEEE/RSJ International Conference on*. IEEE, 2008, pp. 1103–1108.

[38] L. Sentis and O. Khatib, "A whole-body control framework for humanoids operating in human environments," in *Robotics and Automation, 2006. ICRA 2006. Proceedings 2006 IEEE International Conference on*. IEEE, 2006, pp. 2641–2648.

[39] G. Boone and J. Hodgins, "Slipping and tripping reflexes for bipedal robots," *Autonomous Robots*, vol. 4, pp. 259–271, 1997.

[40] K. Kaneko, F. Kanehiro, S. Kajita, M. Morisawa, K. Fujiwara, K. Harada, and H. Hirukawa, "Slip observer for walking on a low friction floor," *Conference on Internation Robots and Systems (IROS)*, pp. 634–640, 2005.

[41] C. Klein and S. Kittivatcharapong, "Optimal force distribution for the legs of a walking machine with friction cone constraints," *IEEE Transactions on Robotics and Automation*, vol. 6, no. 1, pp. 73–85, 1990.

[42] J. Nagle, "Realistic animation of legged running on rough terrain," in *Proceedings Computer Animation*. IEEE, 1995, pp. 154–162.

[43] A. Angelova, L. Matthies, D. Helmick, and P. Perona, "Learning and prediction of slip from visual information," *Journal of Field Robotics*, vol. 24, no. 3, pp. 205–231, 2007.

[44] S. Muller, M. Uchanski, and K. Hedrick, "Estimation of the maximum tire-road friction coefficient," *Journal of dynamic systems, measurement, and control*, vol. 125, p. 607, 2003.

[45] R. Rajamani, D. Piyabongkarn, J. Lew, K. Yi, and G. Phanomchoeng, "Tire-road coefficient estimation, real-time methods for active automotive safety applications," *IEEE Control Systems Magazine*, August 2010.

[46] H. Pacejka and E. Bakker, "The magic formula tyre model," *Vehicle system dynamics*, vol. 21, no. S1, pp. 1–18, 1992.

[47] H. Olsson, K. Åstrom, C. Canudas de Wit, M. Gafvert, and P. Lischinsky, "Friction models and friction compensation," *European journal of control*, vol. 4, pp. 176–195, 1998.

[48] D. Karnopp, "Computer simulation of slip-stick friction in mechanical dynamic systems," *Journal of Dynamic Systems, Measurement, and Control*, vol. 107, no. 1, pp. 100–103, 1985.

[49] B. Armstrong-Hélouvry, P. Dupont, and C. De Wit, "A survey of models, analysis tools and compensation methods for the control of machines with friction," *Automatica*, vol. 30, no. 7, pp. 1083–1138, 1994.

[50] R. Featherstone, *Rigid body dynamics algorithms*. Springer-Verlag New York Inc, 2008.

[51] P. Dahl, "A solid friction model," DTIC Document, Tech. Rep., 1968.

[52] C. Canudas de Wit, H. Olsson, K. Astrom, and P. Lischinsky, "A new model for control of systems with friction," *IEEE Transactions on Automatic Control*, vol. 40, no. 3, pp. 419–425, 1995.

[53] P. Bliman and N. Sorine, "Easy-to-use realistic dry friction models for automatic control," *Proceedings of the Third European Control Conference*, vol. 4, pp. 3788–3794, 1995.

[54] A. Visintin, *Differential models of hysteresis*. Springer Verlag, 1994, vol. 111.

[55] S. Billings and W. Voon, "Least squares parameter estimation algorithms for non-linear systems," *International journal of systems science*, vol. 15, no. 6, pp. 601–615, 1984.

[56] J. Dormand and P. Prince, "A family of embedded Runge-Kutta formulae," *Journal of Computational and Applied Mathematics*, vol. 6, no. 1, pp. 19–26, 1980.

[57] K. Hunt and F. Crossley, "Coefficient of restitution interpreted as damping in vibroimpact," *Journal of Applied Mechanics*, vol. 42, p. 440, 1975.

[58] D. Wight, E. Kubica, and D. Wang, "Introduction of the foot placement estimator: A dynamic measure of balance for bipedal robotics," *Journal of Computational and Nonlinear Dynamics*, vol. 3, p. 011009, 2008.

[59] P. Bibalan and R. Featherstone, "A study of soft contact models in simulink," in *Proceedings of the Australasian Conference on Robotics and Automation (ACRA)*, 2009, pp. 2–4.

[60] O. Khatib, "A unified approach for motion and force control of robot manipulators: The operational space formulation," *IEEE Journal of Robotics and Automation*, vol. 3, no. 1, pp. 43–53, 1987.

[61] S. Hyon, "Compliant terrain adaptation for biped humanoids without measuring ground surface and contact forces," *IEEE Transactions on Robotics*, vol. 25, no. 1, pp. 171–178, 2009.

[62] K. Suwanratchatamanee, M. Matsumoto, and S. Hashimoto, "Haptic sensing foot system for humanoid robot and ground recognition with one leg balance," *IEEE Transactions on Industrial Electronics*, vol. 58, no. 99, pp. 1–1, 2009.

[63] E. Ohashi, T. Sato, and K. Ohnishi, "Motion control of environmental adaptation for biped robot," in *IEEE International Workshop on Advanced Motion Control*. IEEE, 2008, pp. 306–311.

Appendix

Appendix A

Bipedal Robot Equations of Motion

The following model is a 4-DoF bipedal robot with a point mass at the hip to represent the torso. This is a common model for a bipedal robot due to its simplicity. Since the biped foot is not assumed to be fixed to the inertial frame, two more degrees of freedom representing the horizontal and vertical displacement of the biped are required. This results in a total of 6 degrees of freedom.

The equations of motion are derived using Lagrange equations.

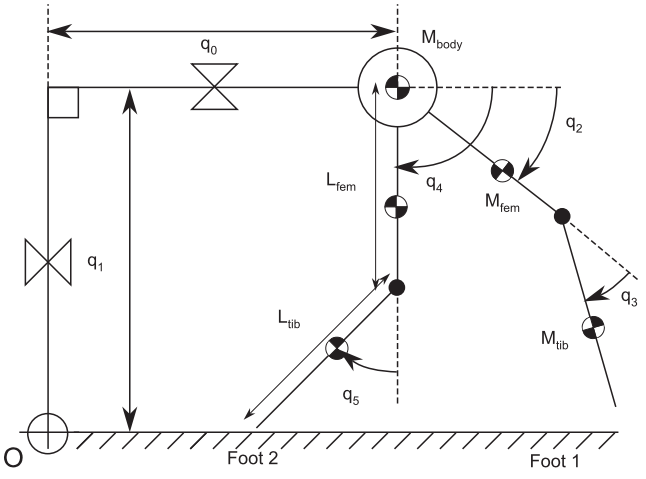

FIGURE A.1: Biped Model with Floating Base

$$M(q)\ddot{q} + C(\dot{q}, q) + G(q) = \tau_i + J_1^T F_1 + J_2^T F_2 \tag{A.1}$$

The Mass Matrix:

$$M(q) = \begin{bmatrix} M_{11} & M_{12} & M_{13} & M_{14} & M_{15} & M_{16} \\ M_{21} & M_{22} & M_{23} & M_{24} & M_{25} & M_{26} \\ M_{31} & M_{32} & M_{33} & M_{34} & M_{35} & M_{36} \\ M_{41} & M_{42} & M_{43} & M_{44} & M_{45} & M_{46} \\ M_{51} & M_{52} & M_{53} & M_{54} & M_{55} & M_{56} \\ M_{61} & M_{62} & M_{63} & M_{64} & M_{65} & M_{66} \end{bmatrix} \tag{A.2}$$

where:

$$M_{11} = M_{body} + 2M_{fem} + 2M_{tib} \tag{A.3}$$

$$M_{12} = 0 \tag{A.4}$$

$$M_{13} = -L_{tib}M_{tib}\sin(q_2 + q_3)/2 - L_{fem}M_{fem}\sin(q_2)/2 - L_{fem}M_{tib}\sin(q_2) \tag{A.5}$$

$$M_{14} = -L_{tib}M_{tib}\sin(q_2 + q_3)/2 \tag{A.6}$$

$$M_{15} = -L_{tib}M_{tib}\sin(q_4 + q_5)/2 - L_{fem}M_{fem}\sin(q_4)/2 - L_{fem}M_{tib}\sin(q_4) \tag{A.7}$$

$$M_{16} = -L_{tib}M_{tib}\sin(q_4 + q_5)/2 \tag{A.8}$$

$$M_{21} = 0 \tag{A.9}$$

$$M_{22} = M_{body} + 2M_{fem} + 2M_{tib} \tag{A.10}$$

$$M_{23} = L_{tib}M_{tib}\cos(q_2 + q_3)/2 + L_{fem}M_{fem}\cos(q_2)/2 + L_{fem}M_{tib}\cos(q_2) \tag{A.11}$$

$$M_{24} = L_{tib}M_{tib}\cos(q_2 + q_3)/2 \tag{A.12}$$

$$M_{25} = L_{tib}M_{tib}\cos(q_4 + q_5)/2 + L_{fem}M_{fem}\cos(q_4)/2 + L_{fem}M_{tib}\cos(q_4) \tag{A.13}$$

$$M_{26} = L_{tib}M_{tib}\cos(q_4 + q_5)/2 \tag{A.14}$$

$$M_{31} = -L_{tib}M_{tib}\sin(q_2 + q_3)/2 - L_{fem}M_{fem}\sin(q_2)/2 - L_{fem}M_{tib}\sin(q_2) \tag{A.15}$$

$$M_{32} = L_{tib}M_{tib}\cos(q_2 + q_3)/2 + L_{fem}M_{fem}\cos(q_2)/2 + L_{fem}M_{tib}\cos(q_2) \tag{A.16}$$

$$M_{33} = I_{fem} + L_{fem}^2M_{fem}/4 + L_{fem}^2M_{tib} + L_{tib}^2M_{tib}/4 + L_{fem}L_{tib}M_{tib}\cos(q_3) \tag{A.17}$$

$$M_{34} = L_{tib}M_{tib}(L_{tib} + 2L_{fem}\cos(q_3))/4 \tag{A.18}$$

$$M_{35} = M_{36} = 0 \tag{A.19}$$

$$M_{41} = -L_{tib}M_{tib}\sin(q_2+q_3)/2 \tag{A.20}$$

$$M_{42} = L_{tib}M_{tib}\cos(q_2+q_3)/2 \tag{A.21}$$

$$M_{43} = L_{tib}M_{tib}(L_{tib}+2L_{fem}\cos(q_3))/4 \tag{A.22}$$

$$M_{44} = M_{tib}L_{tib}^2/4 + I_{tib} \tag{A.23}$$

$$M_{45} = M_{46} = 0 \tag{A.24}$$

$$M_{51} = -L_{tib}M_{tib}\sin(q_4+q_5)/2 - L_{fem}M_{fem}\sin(q_4)/2 - L_{fem}M_{tib}\sin(q_4) \tag{A.25}$$

$$M_{52} = L_{tib}M_{tib}\cos(q_4+q_5)/2 + L_{fem}M_{fem}\cos(q_4)/2 + L_{fem}M_{tib}\cos(q_4) \tag{A.26}$$

$$M_{53} = M_{54} = 0 \tag{A.27}$$

$$M_{55} = I_{fem} + L_{fem}^2M_{fem}/4 + L_{fem}^2M_{tib} + L_{tib}^2M_{tib}/4 + L_{fem}L_{tib}M_{tib}\cos(q_5) \tag{A.28}$$

$$M_{56} = L_{tib}M_{tib}(L_{tib}+2L_{fem}\cos(q_5))/4 \tag{A.29}$$

$$M_{61} = -L_{tib}M_{tib}\sin(q_4+q_5)/2 \tag{A.30}$$

$$M_{62} = L_{tib}M_{tib}\cos(q_4+q_5)/2 \tag{A.31}$$

$$M_{63} = M_{64} = 0 \tag{A.32}$$

$$M_{65} = L_{tib}M_{tib}(L_{tib}+2L_{fem}\cos(q_5))/4 \tag{A.33}$$

$$M_{66} = M_{tib}L_{tib}^2/4 + I_{tib} \tag{A.34}$$

The Coriolis and centrifugal vector B:

$$B(\dot{q},q) = \begin{bmatrix} B_{11} & B_{21} & B_{31} & B_{41} & B_{51} & B_{61} \end{bmatrix}^T \tag{A.35}$$

where:

$$\begin{aligned} B_{11} = &- \dot{q}_3(L_{tib}M_{tib}\dot{q}_2\cos(q_2+q_3)/2 + L_{tib}M_{tib}\dot{q}_3\cos(q_2+q_3)/2) \\ &- \dot{q}_5((L_{tib}M_{tib}\dot{q}_4\cos(q_4+q_5))/2 + L_{tib}M_{tib}\dot{q}_5\cos(q_4+q_5)/2) \\ &-\dot{q}_2(\dot{q}_2(L_{tib}M_{tib}\cos(q_2+q_3)/2 + L_{fem}M_{fem}\cos(q_2)/2 + L_{fem}M_{tib}\cos(q_2)) \\ &\quad + L_{tib}M_{tib}\dot{q}_3\cos(q_2+q_3)/2) \\ &-\dot{q}_4(\dot{q}_4(L_{tib}M_{tib}\cos(q_4+q_5)/2 + L_{fem}M_{fem}\sin(q_4)/2 + L_{fem}M_{tib}\sin(q_4)) \\ &\quad + L_{tib}M_{tib}\dot{q}_5\cos(q_4+q_5)/2) \end{aligned} \tag{A.36}$$

$$\begin{aligned}
B_{21} = &- \dot{q}_3(L_{tib}M_{tib}\dot{q}_2\sin(q_2+q_3)/2 + L_{tib}M_{tib}\dot{q}_3\sin(q_2+q_3)/2) \\
&- \dot{q}_5(L_{tib}M_{tib}\dot{q}_4\sin(q_4+q_5)/2 + L_{tib}M_{tib}\dot{q}_5\sin(q_4+q_5)/2) \\
&-\dot{q}_2(\dot{q}_2(L_{tib}M_{tib}\sin(q_2+q_3)/2 + L_{fem}M_{fem}\sin(q_2)/2 + L_{fem}M_{tib}\sin(q_2)) \\
&\quad + L_{tib}M_{tib}\dot{q}_3\sin(q_2+q_3)/2) \\
&-\dot{q}_4(\dot{q}_4(L_{tib}M_{tib}\sin(q_4+q_5)/2 + L_{fem}M_{fem}\sin(q_4)/2 + L_{fem}M_{tib}\sin(q_4)) \\
&\quad + L_{tib}M_{tib}\dot{q}_5\sin(q_4+q_5)/2)
\end{aligned} \tag{A.37}$$

$$\begin{aligned}
B_{31} = &- \dot{q}_3(L_{fem}L_{tib}M_{tib}\dot{q}_2\sin(q_3)/2 + L_{fem}L_{tib}M_{tib}\dot{q}_3\sin(q_3)/2) \\
&- L_{fem}L_{tib}M_{tib}\dot{q}_2\dot{q}_3\sin(q_3)/2
\end{aligned} \tag{A.38}$$

$$B_{41} = L_{fem}L_{tib}M_{tib}\dot{q}_2^2\sin(q_3)/2 \tag{A.39}$$

$$\begin{aligned}
B_{51} = &- \dot{q}_5(L_{fem}L_{tib}M_{tib}\dot{q}_4\sin(q_5)/2 + (L_{fem}L_{tib}M_{tib}\dot{q}_5\sin(q_5))/2) \\
&- L_{fem}L_{tib}M_{tib}\dot{q}_4\dot{q}_5\sin(q_5)/2
\end{aligned} \tag{A.40}$$

$$B_{61} = L_{fem}L_{tib}M_{tib}\dot{q}_4^2\sin(q_5)/2 \tag{A.41}$$

The gravity vector G:

$$G(q) = \begin{bmatrix}
0 \\
g(M_{body} + 2M_{fem} + 2M_{tib}) \\
g(L_{tib}M_{tib}\cos(q_2+q_3) + L_{fem}M_{fem}\cos(q_2) + 2L_{fem}M_{tib}\cos(q_2))/2 \\
gL_{tib}M_{tib}\cos(q_2+q_3)/2 \\
g(L_{tib}M_{tib}\cos(q_4+q_5) + L_{fem}M_{fem}\cos(q_4) + 2L_{fem}M_{tib}\cos(q_4))/2 \\
gL_{tib}M_{tib}\cos(q_4+q_5)/2
\end{bmatrix} \tag{A.42}$$

where g is the acceleration due to gravity.

The jacobian matrix to Foot 1 J_1:

$$J_1(q) = \begin{bmatrix} 1 & 0 & -L_{fem}\sin(q_2) - L_{tib}\sin(q_2+q_3) & -L_{tib}\sin(q_2+q_3) & 0 & 0 \\ 0 & 1 & L_{fem}\cos(q_2) + L_{tib}\cos(q_2+q_3) & L_{tib}\cos(q_2+q_3) & 0 & 0 \\ 0 & 0 & 1 & 1 & 0 & 0 \end{bmatrix} \tag{A.43}$$

The jacobian matrix to Foot 2 J_2:

$$J_2(q) = \begin{bmatrix} 1 & 0 & 0 & 0 & -L_{fem}\sin(q_4) - L_{tib}\sin(q_4+q_5) & -L_{tib}\sin(q_4+q_5) \\ 0 & 1 & 0 & 0 & L_{fem}\cos(q_4) + L_{tib}\cos(q_4+q_5) & L_{tib}\cos(q_4+q_5) \\ 0 & 0 & 0 & 0 & 1 & 1 \end{bmatrix} \tag{A.44}$$